Hindawi
Advances in Civil Engineering
Volume 2019, Article ID 3858457, 22 pages
https://doi.org/10.1155/2019/3858457

Research Article

Optimal Seismic Intensity Measure Selection for Isolated Bridges under Pulse-Like Ground Motions

Linwei Jiang,[1] Jian Zhong,[1] Min He,[1] and Wancheng Yuan[2]

[1]*Department of Civil Engineering, Hefei University of Technology, Hefei 230009, China*
[2]*State Key Laboratory of Disaster Reduction in Civil Engineering, Tongji University, Shanghai 200092, China*

Correspondence should be addressed to Jian Zhong; jzhong@hfut.edu.cn

Received 22 July 2019; Revised 27 October 2019; Accepted 14 November 2019; Published 30 December 2019

Academic Editor: Annan Zhou

Isolated bridges are commonly designed in the near-fault region to balance excessive displacement and seismic force. Optimal intensity measures (IMs) of probabilistic seismic demand models for isolated bridges subjected to pulse-like ground motions are identified in this study. Four typical isolated girder bridge types with varied pier height (from 4 m to 20 m) are employed to conduct the nonlinear time history analysis. Totally seven structure-independent IMs are considered and compared. Critical engineering demand parameters (EDPs), namely, pier ductility demands and bearing deformation along the longitudinal and transverse directions, are recorded during the process. In general, PGV tends to be the optimal IM for isolated bridges under pulse-like ground motions based on practicality, efficiency, proficiency, and sufficiency criterions. The results can offer effective guidance for the optimal intensity measure selection of the probabilistic seismic demand models (PSDMs) of isolated bridges under pulse-like ground motions.

1. Introduction

It has been observed that ground motion recordings in the near-fault region, which is usually taken as within 20 km from the fault rupture, tend to differ from far-field rivals in three main characteristics, that is, velocity pulse, directivity effect, and large vertical acceleration component [1]. Some of these differences are usually shown in the velocity and displacement time series, which have been attributed to two effects: the rupture directivity effect and the fling step. The rupture directivity denotes the effect of rupture propagation relative to the site [2]. The near-fault directivity often manifests in the fault-normal direction, which is the direction perpendicular to the surface of the fault rupture. A site may experience forward directivity when the rupture propagates towards the site with a velocity almost equal to the shear-wave velocity of the soil. This effect appears in the form of a large, long-period velocity pulse. And the fling step effect is observed in the fault-parallel direction, that is, the direction paralleled to the fault slip, which appears in the form of a permanent displacement. Due to the above features, the near-fault ground motions impose high input energy on structures and result in severe damage. This phenomenon was originally discovered by Bertero et al. [3, 4]. However, it is only after the 1994 Northridge earthquake that the severe effect of near-fault ground motions on the demand of structures and the necessity of incorporating the effect into the design process were recognized [5, 6].

The probabilistic seismic demand models conditioned on a single intensity measure (IM) of ground motions are a common and necessary step in generating the analytical fragility curves. The intensity measures (IMs) represent characteristics of ground motions and play an important role in the probabilistic seismic demand analysis. Tracking and reducing uncertainty associated with the PSDM can be accomplished by selecting an optimal IM upon which the demand models are conditioning [7].

Researchers have done a lot of work on the selection of optimal IMs for far-field ground motions in the recent years. The Modified Mercalli Intensity Scale was chosen by the Applied Technology Council [8] as the preferred IM. These

data were adopted in the risk assessment software package HAZUS. The recent versions of HAZUS selected the spectral acceleration at a period of 1 s (S_{a-1}) and peak ground displacement (PGD) as the IMs. Padgett et al. [7] investigated the seismic response of the multispan simply supported steel girder bridge class and found that peak ground acceleration (PGA) and spectral acceleration at the fundamental period (S_a) tended to be the most optimal IMs for synthetic ground motions and cumulative absolute velocity was also a contender for recorded motions. In addition to the common IMs, more complex parameters, multiparameter, or vector-based IMs have been proposed [9–12]. Within the bridge engineering community, PGA and S_a are the widely accepted IMs [7, 13].

However, there is relatively less research on the optimal intensity measures of pulse-like ground motions [14]. Yakhchalian et al. [15] proposed that the commonly used scalar intensity measure, namely, the spectral acceleration at the fundamental period of the structure (S_a), is deficient and insufficient to predict the seismic response with respect to the pulse periods of pulse-like ground motions and developed an optimal integral-based IM (I-S_a) with 15 generic frame structures. Baker and Cornell [16] demonstrated that the near-fault pulse-like ground motions are not well described by traditional intensity measures and proposed a vector intensity measure that combines S_a with a measure of the spectral shape. Li et al. [17] proposed two fuzzy-valued (F_V) structure-specific intensity measures (one is based on the squared spectral velocity and the other is based on the inelastic spectral displacement) to characterize near-fault pulse-like ground motions. Zhong et al. [1] investigated the response of cable-stayed bridges under synthetic and recorded pulse-like ground motions and found that PGV tends to be the optimal intensity measure compared to other six structure-independent IMs.

In general, the existing IMs can be classified into two categories, that is, structure-dependent IMs and structure-independent IMs. The former combine structure characteristics with intensity measures, while the latter only consider the features of ground motions. However, Padgett et al. [7] proposed that structure-dependent IMs are difficult to obtain in a regional risk assessment for bridge portfolios due to the lack of sufficient information such as fundamental periods of structures. Isolated bridges display totally different seismic response compared to the ordinary short period bridges. Consequently, this study aims to identify the optimal IM for isolated bridges under pulse-like ground motions by evaluating seven existing structure-independent IMs. Four typical isolated bridge types with varied pier height (from 4 m to 20 m) are employed to conduct the nonlinear time history analysis. Efficiency, practicality, proficiency and sufficiency, and hazard computability are selected to evaluate the candidate intensity measures.

2. Fragility Function Methodology

As an emerging tool, the seismic fragility is a useful tool for evaluating the potential seismic damage of bridges during the earthquakes. Seismic fragility refers to the conditional probability that the seismic demand meets or exceeds the seismic capacity of structures subjected to a series of specific ground motions, generally expressed in equation (1):

$$P_{\text{vulnerability}} = P\left(S_D \geq S_C \mid \text{IM}\right) = 1 - \Phi\left(\frac{\ln\left(S_D/S_C\right)}{\sqrt{\beta_{D|\text{IM}}^2 + \beta_C^2}}\right), \tag{1}$$

where $P_{\text{vulnerability}}$ is the conditional failure probability, S_D and $\beta_{D|\text{IM}}$ are the median and dispersion of seismic demand, respectively, S_C and β_c are the corresponding median and dispersion of seismic capacity, respectively, and $\Phi(\cdot)$ is the cumulative normal distribution function. In this paper, probabilistic seismic demand analysis (PSDA) is utilized to derive the fragility curves of bridges, which can establish the probabilistic relationship between the engineering demand parameters (EDPs) of components and the ground motion intensity measures (IMs) [18]. During the process, the peak demands (D_i) of the critical components, namely, the curvature ductility of the pier and deformation of the bearing, are recorded for the ith ground motion.

If it is assumed that the seismic demand coincides with the lognormal distribution, the relationship between the median of seismic demand (S_D) and the intensity measure (IM) can be written in equation (2):

$$\begin{aligned} S_D &= a\text{IM}^b, \\ \text{or } \ln\left(S_D\right) &= \ln a + b\ln\left(\text{IM}\right), \end{aligned} \tag{2}$$

where a and b are regression coefficients obtained from the response data of the nonlinear time history analysis. The dispersion $\beta_{D|\text{IM}}$ is theoretically related to ground motions. But, for the sake of simplification, it is usually assumed that $\beta_{D|\text{IM}}$ is constant [19] as follows:

$$\beta_{D|\text{IM}} = \sqrt{\frac{\sum_{i=1}^{n}\left[\ln\left(D_i\right) - \ln\left(S_D\right)\right]^2}{n-2}}, \tag{3}$$

where n is the number of ground motions.

3. Characteristics of an Optimal IM

Selection of an approximate IM plays a vital role in the probabilistic demand seismic models, which provides the link between EDPs and IMs. An optimal IM should satisfy the following five requirements [1, 7].

3.1. Practicality. Practicality is used to examine the correlation between the demands placed on the structure and the intensity measures of ground motions, which is measured by the regression parameter b in equation (2). A larger value of b indicates a more practical IM.

3.2. Efficiency. Efficiency is known as the common metric that characterizes an optimal IM. An efficient IM can reduce the variation in the estimated demand median, which is represented by the lower regression parameter $\beta_{D|\text{IM}}$ in equation (3).

3.3. Proficiency: A Composite Metric of Efficiency and Practicality. The conventional selection of an optimal IM based on practicality and efficiency may lead to a challenge in balancing the two parameters. To deal with the problem, Padgett et al. [7] proposed a composite measure ζ to combine practicality and efficiency, which is defined in equation (4). A more proficient IM yields a lower ζ.

$$\zeta = \frac{\beta_{\mathrm{D|IM}}}{b}. \tag{4}$$

3.4. Sufficiency. Sufficiency is an alternative measure to identify an optimal IM of PSDMs [19]. A sufficient IM is statistically independent of ground motion characteristics, such as the magnitude (M), the epicentral distance (R), and fault characteristics. The sufficiency of IMs is assessed with a regression analysis on the residual ε/IM to obtain the corresponding p value, from the PSDM to the ground motion characteristics, M or R [1]. A larger p value of the regression evaluation indicates a more sufficient IM.

3.5. Hazard Computability. Hazard computability is also a viable measure of an optimal IM. As defined in Giovenale et al. [20], the hazard computability is the level of effort to assess the seismic hazard or derive the hazard curve. PGA or spectral accelerations at the period of 0.2 s or 1 s are readily available in hazard maps; however, other structure-dependent IMs need even more effort and there is difficulty in calculating some IMs from hazard maps.

Therefore, only structure-independent IMs, namely, seven existing IMs in Padgett et al. [7], are considered and compared in this paper. The detailed IMs are listed in Table 1 with their formulas.

4. Characteristics and Modeling of Isolated Bridges

Four typical isolated girder bridge types that are common in transportation networks are adopted in this paper as case studies, namely, multicell box girder (MCBG), multibeam box girder (MBBG), concrete I-girder bridge (CIGB), and steel I-girder bridge (SIGB). To generate PSDMs that are representative of each bridge type, some generalizations of the configurations are necessary to be made. As-built bridge data are collected from the various departments of transportation and the advice of engineers who are experienced in designing and restoring bridges is taken to determine pier details, superstructure geometry, isolation bearing parameters, and so forth. The Guidelines for Seismic Design of Highway Bridges [21] are also referred to in order to ensure that the crucial characteristics (e.g., stiffness, mass, and natural period) are generally consistent with the existing bridges. In particular, the pier dimension is determined to guarantee that the axial compression ratio of piers is about 10% for the ductility demand. In this way, the conclusion obtained in this paper is representative of the isolated girder bridge types rather than a certain bridge (Figure 1).

Table 1: List of intensity measures compared in this paper.

IMs	Description	Equation	Units
PGA	Peak ground acceleration	$\max\lvert a(t)\rvert$	g
PGV	Peak ground velocity	$\max\lvert v(t)\rvert$	m/s
PGD	Peak ground displacement	$\max\lvert d(t)\rvert$	m
CAV	Cumulative absolute velocity	$\int_0^{t_{\max}} \lvert a(t)\rvert \mathrm{d}t$	m/s
CAD	Cumulative absolute displacement	$\int_0^{t_{\max}} \lvert v(t)\rvert \mathrm{d}t$	m
Ia	Arias intensity	$(\pi/2g)\int_0^{t_{\max}} [a(t)]^2 \mathrm{d}t$	m/s
Iv	Velocity intensity	$(\pi/2g)\int_0^{t_{\max}} [v(t)]^2 \mathrm{d}t$	m

To demonstrate the effect of structure periods on the optimized results, the pier height varies from 4 m to 20 m to generate a wide period range. The typical longitudinal layout of the bridge is given in Figure 2. The vertical reinforcement ratio of the piers is set as 1.2% uniformly with 16 mm circular ties spaced at 100 mm vertically. The configuration of the pier is also presented in Figure 2, where n is 7 for CIGB and MBBG, 9 for MCBG, and 5 for SIGB and D refers to the side length of the pier. The detailed geometry of each bridge type is summarized in Table 2.

As an effective measure for earthquake resistance and disaster prevention, isolation devices play a vital role in reducing the seismic response of structures. The common types of isolation devices applied in transportation networks include elastomeric bearings (ERB), lead-rubber bearings (LRB), and friction pendulum systems (FPS) [22]. In this paper, LRB is selected to be equipped in the bridge systems. The mechanical properties of LRB can be modeled with a bilinear relationship, which are decided with three parameters, namely, characteristic strength Q, elastic stiffness K_1, and postyielding stiffness K_2. The specific formulas of these parameters are given in Table 3, where A_{lead} is the cross section area of the lead core, G is the shear modulus of the rubber, A is the area of rubber, and Σt_{r} is the total thickness of rubber layers. Since the parameters rely on the specific site scenarios and there is an available LRB portfolio [23], the bearing parameters are determined directly according to the superstructure gravity, which are listed in Table 4.

The four bridge types considered in this paper include elements that would undergo highly nonlinear behavior under earthquakes, which are incorporated into the three-dimensional detailed nonlinear OpenSees models [24]. The superstructure usually remains elastic subjected to the earthquakes and is simulated with elastic beam-column elements. Due to the constraint effect of stirrups in the piers, we should divide the concrete into cover parts and confined parts, respectively. Therefore, we adopt fiber elements to model the substructures. Each fiber element has its own stress-strain relationship and can simulate the confined concrete, cover concrete, and longitudinal reinforcement, respectively. The response of isolation devices is simulated by a nonlinear bilinear element to account for the yielding of lead. Figure 3 gives the schematic of the analytical model of isolated girder bridges with the reinforcement, concrete, and LRB relationships, where σ_{y}, ε_{y}, f_{c}, $\varepsilon_{\mathrm{uu}}$, $\varepsilon_{\mathrm{cu}}$, and K are yield strength, yield strain, compressive strength, strain at

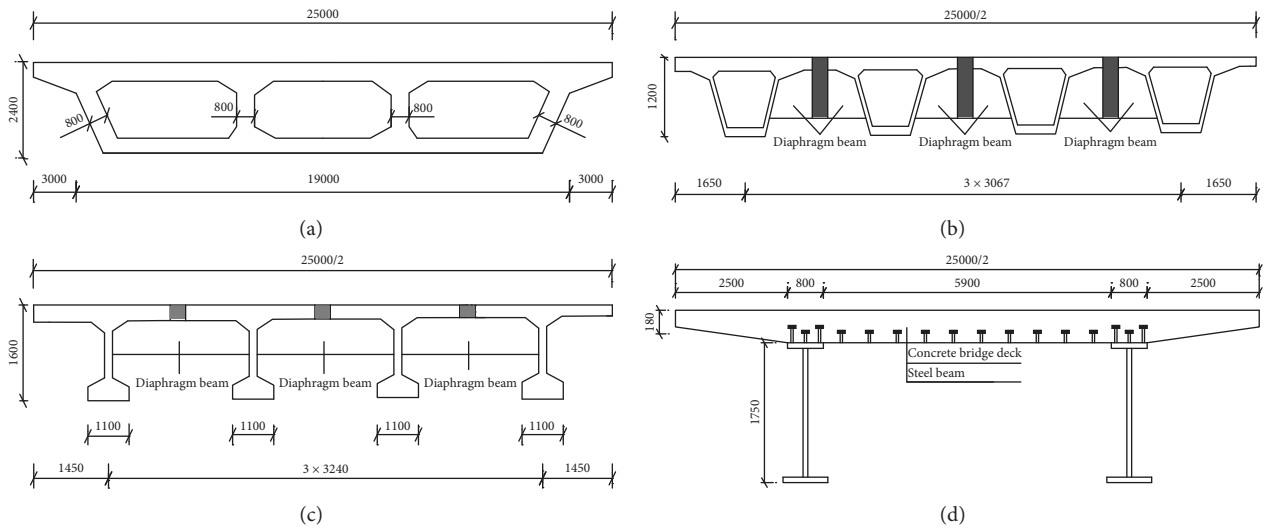

Figure 1: Typical beam cross sections of (a) MCBG, (b) MBBG, (c) CIGB, and (d) SIGB (unit: mm).

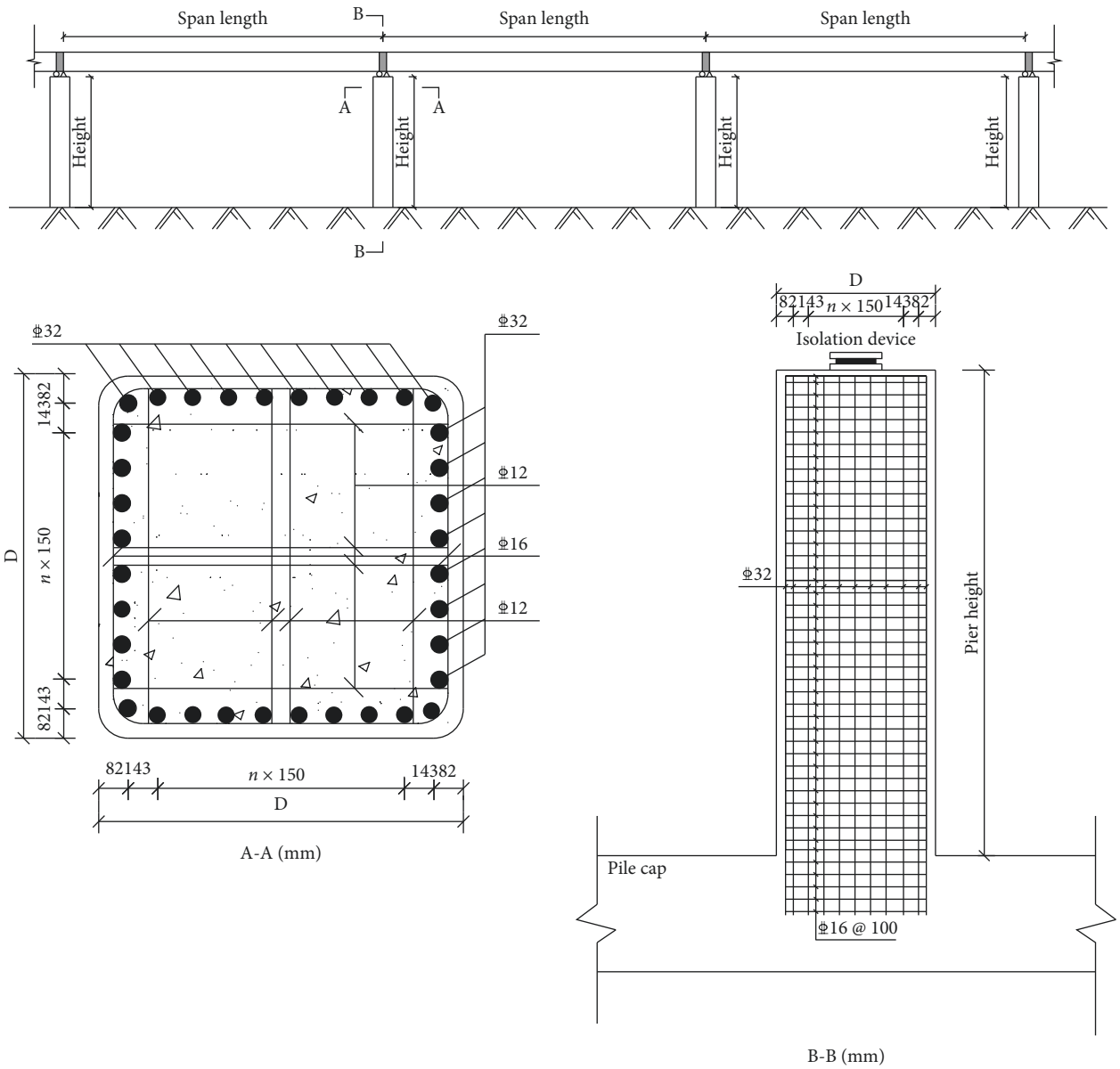

Figure 2: Elevation and pier section properties of simply supported girder bridge.

Table 2: Characteristics of the four isolated girder bridge types.

Bridge type	Height (m)	Column section size (m)	Span length (m)	First order period (s)	Rayleigh damping parameters	
					α_0	α_1
MCBG	4	1.8 × 1.8	35	0.80	0.3927	0.0064
	6			0.84	0.3762	0.0066
	8			0.91	0.3471	0.0072
	10			1.02	0.3110	0.0080
	12			1.17	0.2720	0.0092
	14			1.35	0.2362	0.0106
	16			1.56	0.2047	0.0122
	18			1.8	0.1775	0.0141
	20			2.06	0.1551	0.0161
MBBG	4	1.5 × 1.5	30	0.71	1.7453	0.0014
	6			0.76	1.1635	0.0017
	8			0.83	0.8055	0.0019
	10			0.94	0.6100	0.0020
	12			1.09	0.4760	0.0022
	14			1.28	0.3762	0.0029
	16			1.49	0.3050	0.0037
	18			1.74	0.2513	0.0048
	20			2.00	0.2130	0.0058
CIGB	4	1.5 × 1.5	25	0.54	2.0943	0.0011
	6			0.58	1.3368	0.0013
	8			0.67	0.9240	0.0015
	10			0.78	0.6829	0.0017
	12			0.94	0.5150	0.0022
	14			1.12	0.4054	0.0029
	16			1.33	0.3272	0.0037
	18			1.56	0.2720	0.0046
	20			1.82	0.2293	0.0057
SIGB	4	1.2 × 1.2	35	0.57	0.5511	0.0045
	6			0.64	0.4947	0.0051
	8			0.75	0.4245	0.0059
	10			0.91	0.3491	0.0072
	12			1.11	0.2964	0.0084
	14			1.35	0.2371	0.0105
	16			1.62	0.1976	0.0126
	18			1.91	0.1675	0.0149
	20			2.23	0.1434	0.0174

Table 3: Formulas of the mechanical parameters of LRB.

Parameter	Elastic stiffness K_1	Postyielding stiffness K_2	Characteristic strength Q
LRB	$K_1 = (15\sim30)K_2$	$K_2 = (1.15\sim1.20)\mathrm{GA}/\Sigma t_r$	$Q = f_y A_{lead}$

Table 4: Mechanical properties of LRB of the four bridge types.

Bridge type	Q (kN)	K_1 (kN/m)	K_2 (kN/m)
MCBG	384	28400	4544
MBBG	193	16400	2624
CIGB	171	24700	3952
SIGB	96	14500	2320

compressive strength for unconfined concrete, strain at compressive strength for confined concrete, and amplification factor due to constraint effect, respectively.

In the model, the yield strength, strain-hardening ratio, and elasticity modulus of steel are 400 MPa, 0.5%, and 2.0 × 105 MPa, respectively. With Concrete01 and Steel01 material models in OpenSees, a modified uniaxial Kent-Scott-Park [25] core concrete model is established considering the degraded unloading/reloading stiffness. The compressive strengths of core concrete and cover concrete are set as 29.8 MPa and 26.8 MPa, respectively, and the crushing strains are 0.016 and 0.0035.

In addition, the damping is taken into account for each sample in this paper. The common damping used for structure dynamic analysis includes viscous damping, modal damping, and structure damping [26, 27]. Although many damping models have been proposed, the ideal damping is still difficult to be determined. In this paper, viscous damping is taken into consideration with Rayleigh damping. Rayleigh damping has the characteristics of algebraic

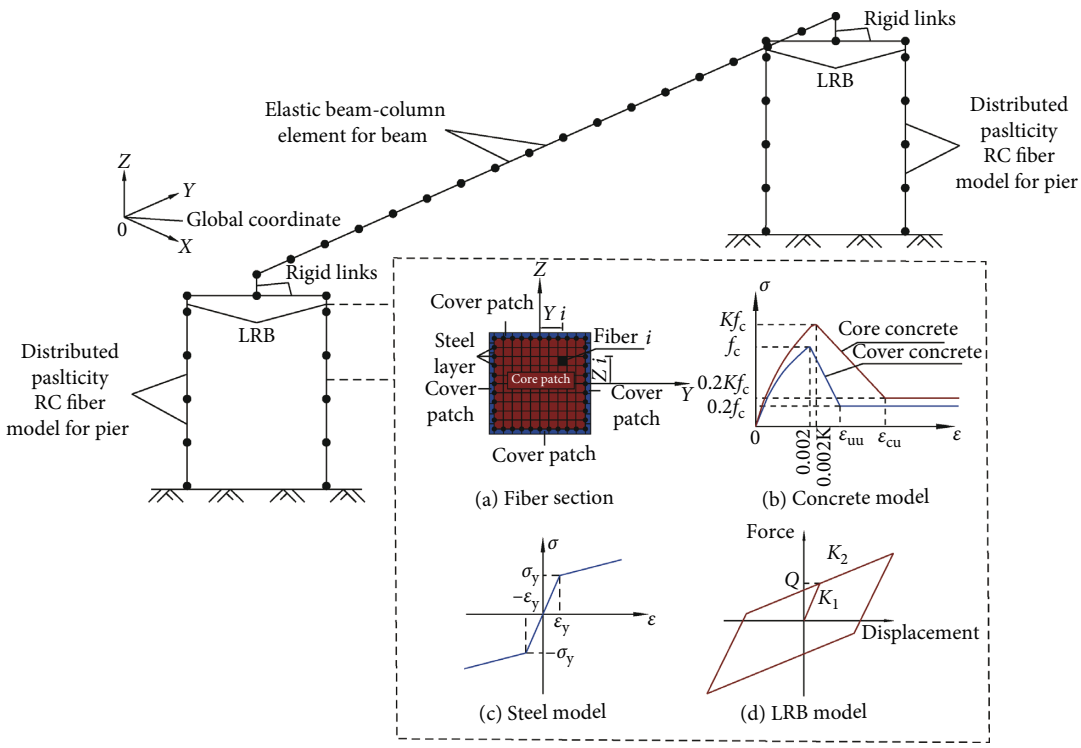

Figure 3: Nonlinear analytical model with models of materials and isolation devices.

manipulation, uniform mathematic expression, and easy application, which is applied widely in structural dynamic response analysis. It is assumed that the damping matrix $[C]$ is the combination of mass matrix $[M]$ and stiffness matrix $[K]$ [26]:

$$[C] = \alpha_0 [M] + \alpha_1 [K], \tag{5}$$

where α_0 and α_1 are two proportionality coefficients calculated from equation (6):

$$\begin{Bmatrix} \alpha_0 \\ \alpha_1 \end{Bmatrix} = \frac{2\xi}{\omega_i + \omega_j} \begin{Bmatrix} \omega_i \omega_j \\ 1 \end{Bmatrix}, \tag{6}$$

where ξ is the damping ratio (assumed as 0.05 in this paper) and ω_i and ω_j are the natural vibration frequencies of structures. Since both the longitudinal and transverse seismic responses of bridges are the focus of this paper, the first two-order longitudinal and transverse frequencies are selected as the values of ω_i and ω_j. The detailed calculation results of Rayleigh damping are given in Table 1.

5. Ground Motion Database

A database consisting of 243 pulse-like ground motions was established by Shahi and Baker [28] in the June 2012 version of the NGA-West2 database by rotating the ground motions and identifying pulses in all orientations. Dabaghi and Kiureghian [29] selected 121 pulse-like ground motions from the database excluding the aftershocks and the records at sites far from the fault (larger than 30 km). Therefore, the remaining pulse-like ground motions database contains 121 pairs in the 2014 version of NGA-West2 database. Figure 4 shows the distribution of pulse-like ground motions with respect to M and R, PGA, PGV, and the pulse period (T_p). The ground motions were recorded from earthquakes, where M ranges from 5.4 to 7.9 and R changes from 0.07 to 28.04 km. The mechanisms of the fault include reverse, strike slip, and reverse oblique. Each record in the pulse-like ground motion database is rotated into the direction containing the largest pulse amplitude and the corresponding orthogonal horizontal direction following the method proposed by Baker [2] and Dabaghi and Kiureghian [29].

In this paper, the nonlinear history analysis is conducted using the abovementioned 121 pairs of pulse-like ground motions. EDPs including curvature ductility demands (μ_x and μ_y: the subscripts x and y refer to the longitudinal and transverse directions), bearing deformation at the pier (δ_x, δ_y), are tracked and recorded during the process.

With the seismic demands and IMs of ground motions, PSDMs are easily developed. For illustration purpose, PSDMs for curvature ductility μ_x conditioned on PGA and PGV of MCBG (pier height is 18 m) are given in Figure 5, where R^2 is the correlation coefficient. As illustrated in the figure, b values are 0.84 and 1.81, respectively, and $\beta_{D|IM}$ are 1.42 and 0.93, which indicates that PGV is more practical and efficient. The corresponding ζ are 1.69 and 0.51, respectively, demonstrating that the more proficient IM is PGV. The sufficiency of PGA is examined with conditional statistical dependence on M and R, which is plotted in Figure 6. As shown in the figure, the p values are 0.2527 and 2.3308×10^{-4} with respect to M and R, respectively. This phenomenon reveals that PGV is more independent of M and dependent on R.

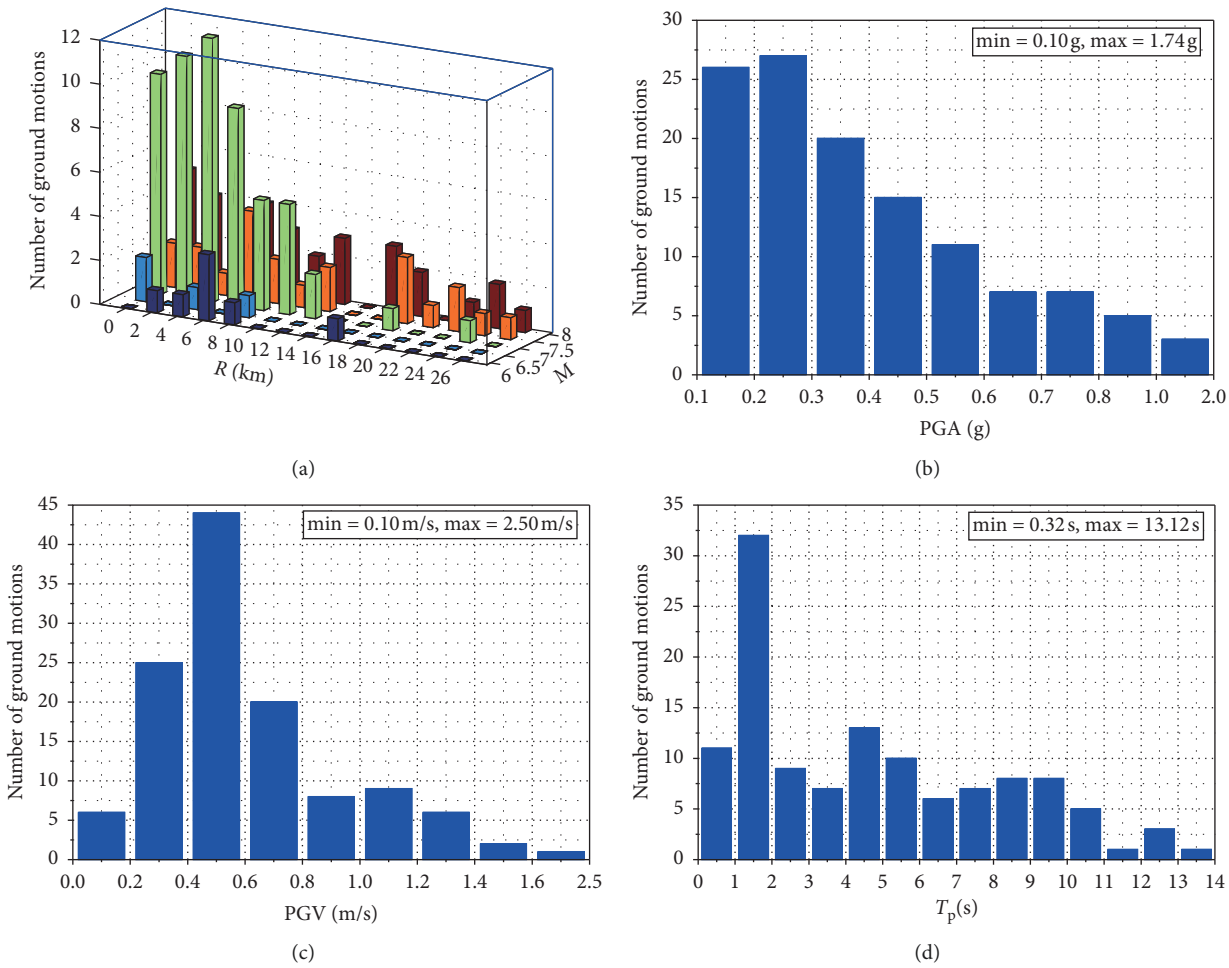

Figure 4: Distribution of pulse-like ground motions with respect to (a) magnitude and source-to-site distance, (b) PGA, (c) PGV, and (d) pulse period T_p.

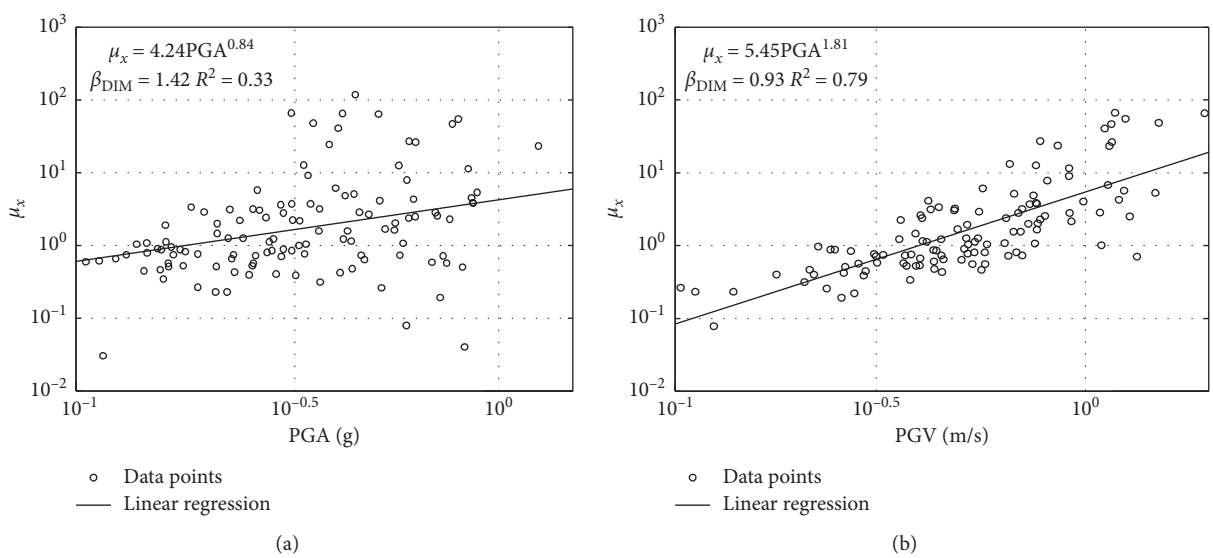

Figure 5: PSDMs for the curvature ductility demand μ_x conditioned on (a) PGA and (b) PGV.

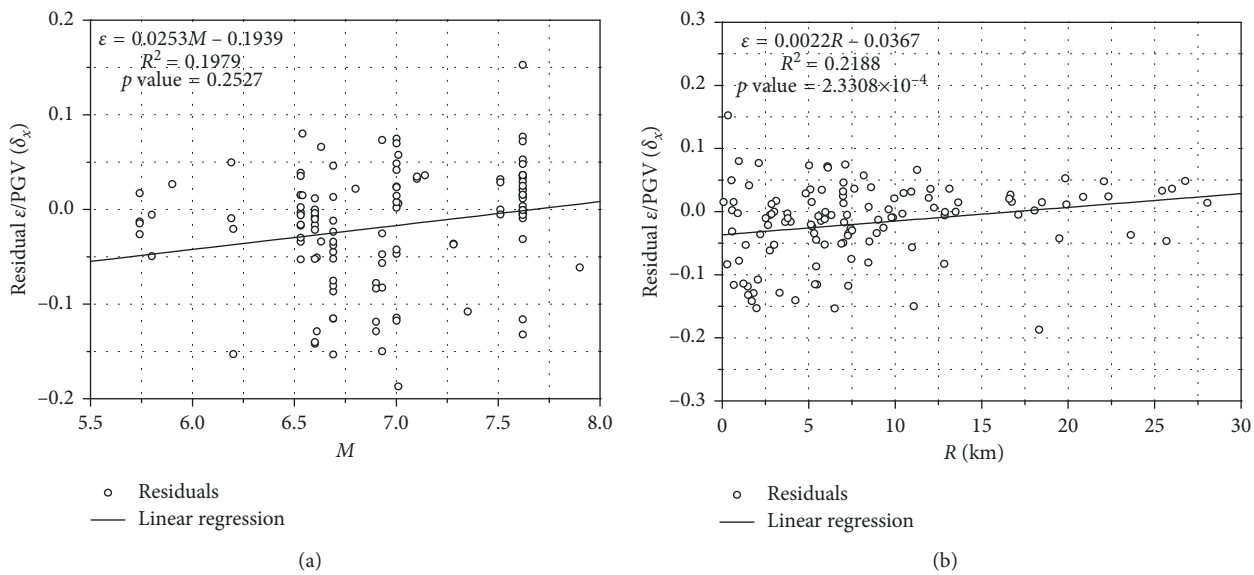

Figure 6: Sufficiency examination of PGV with conditional statistical dependence on (a) M and (b) R.

To highlight the pulse effect on the seismic demand of structures, the optimal intensity measure selection process is repeated for far-field ground motions case. A set of 80 far-field ground motions in Shafieezadeh et al. [30] is used in this paper as the seismic excitation. Figure 7 shows the distribution of far-field ground motions. The ground motions were recorded from earthquakes with M ranging from 5.5 to 7 and R varying from 12.3 to 60 km.

6. Optimal Intensity Measure under Pulse-Like Ground Motions

6.1. Practicality. The practicality comparison of IMs can be estimated with the regression parameter b. A more practical IM yields a larger b. The practicality comparison of the four bridge types with different pier heights is shown in Figures 8 and 9. As illustrated in the figures, PGV tends to be the most practical IM for the pier curvature ductility in the longitudinal and transverse directions, followed by CAV. In contrast, for the lower height cases (from 4 m to 12 m), Iv tends to be the least practical IM, and for the higher height cases (from 14 m to 20 m), PGA is the least practical IM. For the whole height range, Iv, PGD, CAD, and PGA are less appropriate due to relatively low practicality parameter b. Similarly, for the displacement-related EDPs, namely, the bearing displacements, PGV is the most practical in the longitudinal and transverse directions, followed by CAV; the least practical IM is Iv. For the considered height range, Iv, CAD, and PGD tend to be less appropriate because of the relatively low practicality parameter b. In general, PGV tends to be the most practical IM, followed by CAV. In particular, one should notice that, for the long-period cases (e.g., 16–20 m), PGA is not a practical IM under pulse-like ground motions, which is a commonly used IM to establish the analytical fragility curves [22].

As mentioned above, the optimal intensity measure subjected to far-field ground motions is also identified in this paper. Table 5 summarizes the practicality comparison of the seven structure-independent IMs under far-field ground motions of MCBG. For simplicity, the comparison in the transverse direction is not given because it follows a similar tendency. The practicality comparison results of the other three bridge types are also not listed here due to a similar tendency. As shown in the table, CAV tends to be the most practical IM, followed by PGV; however, Iv tends to be the least practical. To demonstrate the pulse effect on the practicality comparison results graphically, Figure 10 shows the comparison results under pulse-like ground motions and far-field ground motions, where PGA, PGV, Iv, and CAV are chosen as the candidate IMs (conditioning on μ_y, the other cases follow the similar tendency). As shown in the figure, PGV can be chosen as the appropriate IM to assess the seismic demand under far-field and pulse-like ground motions. In addition, PGA is less appropriate to develop PSDMs with respect to practicality, especially for higher piers (larger than 16 m) under pulse-like ground motions. For example, b values are 0.69 and 0.35 for 8 m and 16 m cases subject to pulse-like ground motions, respectively, and, for far-field ground motions, b varies in a narrow range. This phenomenon reveals that PGA should not be chosen as the IM for long-period structures under pulse-like ground motions.

6.2. Efficiency. As indicated, the efficiency of IMs can be evaluated with the dispersion $\beta_{D|IM}$ obtained from the PSDMs. The larger $\beta_{D|IM}$ is, the less efficient IM is. Figures 11 and 12 present the efficiency comparison of the four bridge types under pulse-like ground motions. As illustrated in the figures, PGV tends to be the most efficient IM with the pier height ranging from 4 m to 16 m for the pier curvature ductility. However, when the height is 18 m or 20 m, Iv tends to be the most efficient IM. For the bearing deformation, Ia tends to be the most efficient in the longitudinal direction and PGV is the most efficient IM in the transverse direction.

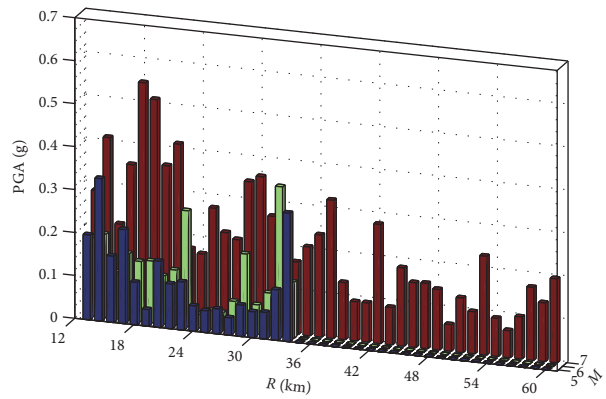

Figure 7: Distribution of far-field ground motions.

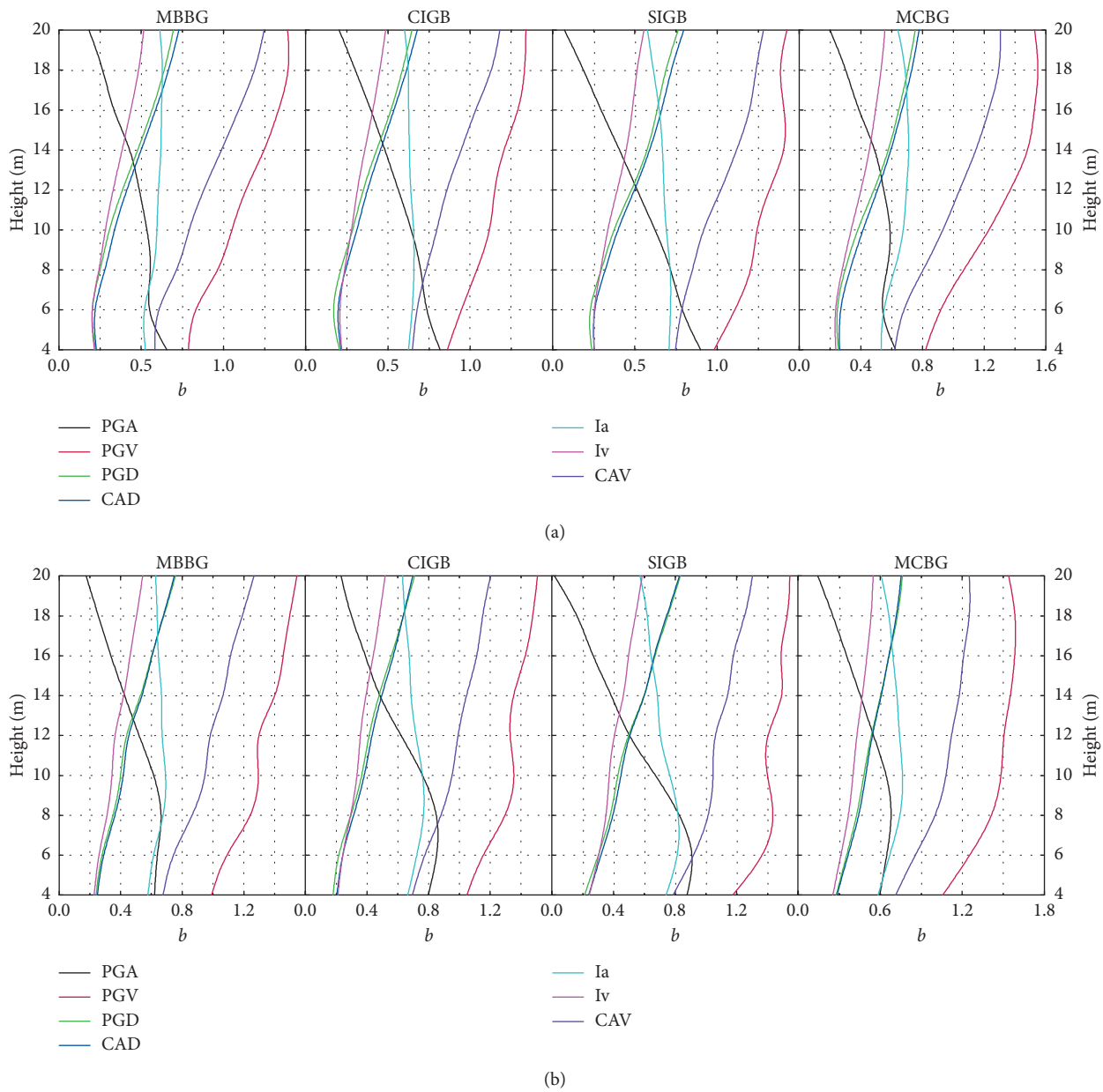

Figure 8: IMs practicality comparison for (a) the pier curvature ductility along the longitudinal direction and (b) the pier curvature ductility along the transverse direction.

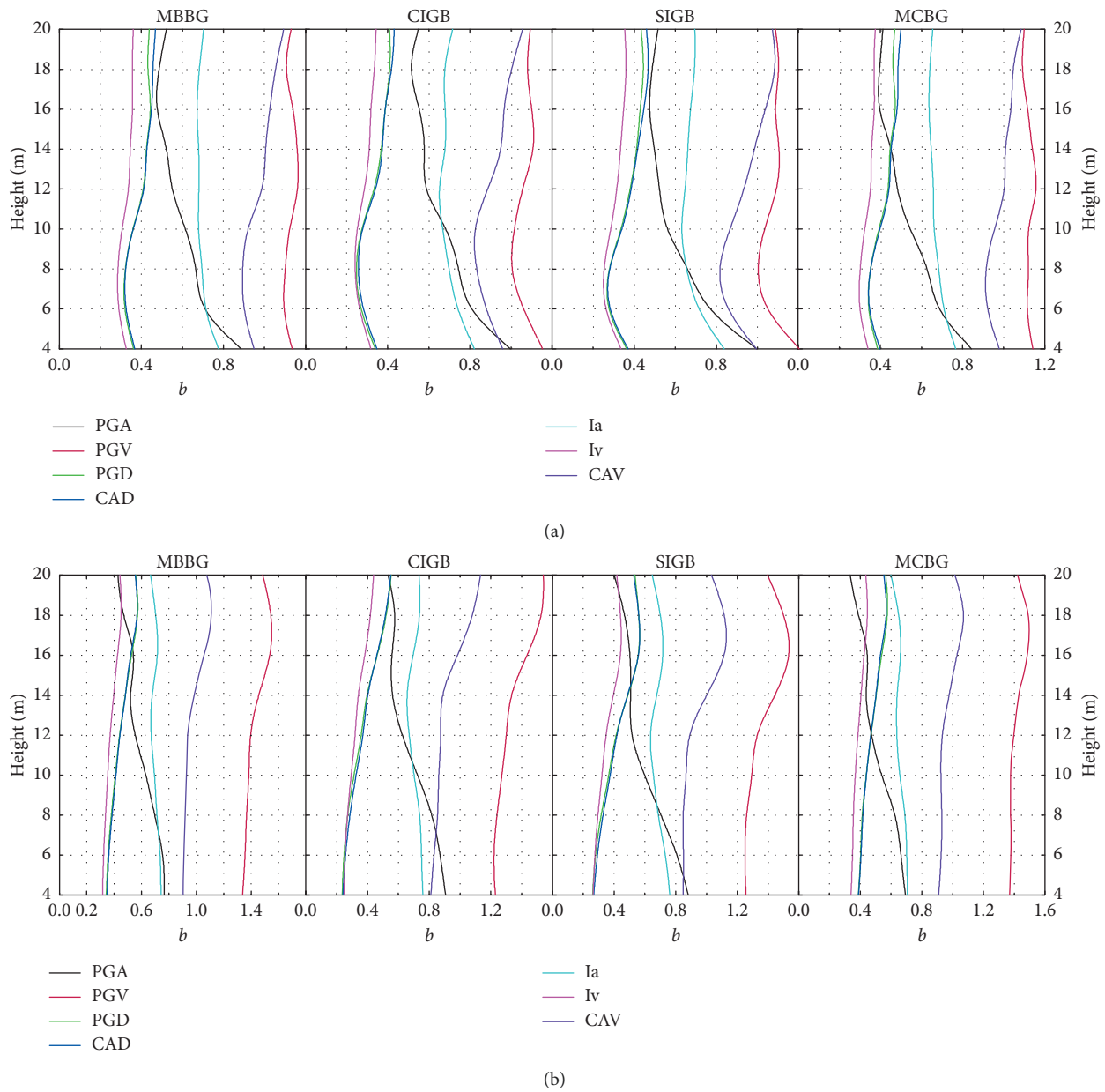

Figure 9: IMs practicality comparison for (a) the bearing deformation along the longitudinal direction and (b) the bearing deformation along the transverse direction.

Table 5: Demand models and practicality comparison of IMs subjected to far-field ground motions.

Height (m)	μ_x							δ_x						
	PGA	PGV	PGD	CAD	Ia	Iv	CAV	PGA	PGV	PGD	CAD	Ia	Iv	CAV
4	0.35	0.37	0.25	0.34	0.23	0.19	**0.45**	0.79	0.82	0.50	0.71	0.47	0.41	**0.91**
6	0.41	0.42	0.20	0.36	0.27	0.21	**0.54**	0.70	0.77	0.40	0.62	0.46	0.37	**0.90**
8	0.45	0.52	0.26	0.45	0.30	0.26	**0.63**	0.73	0.82	0.42	0.66	0.48	0.39	**0.94**
10	0.43	0.53	0.30	0.49	0.30	0.27	**0.64**	0.70	0.81	0.44	0.67	0.47	0.40	**0.94**
12	0.54	0.64	0.37	0.58	0.37	0.33	**0.79**	0.76	0.83	0.46	0.72	0.50	0.42	**1.00**
14	0.66	0.79	0.47	0.70	0.44	0.40	**0.92**	0.76	0.86	0.51	0.76	0.50	0.44	**1.03**
16	0.68	0.85	0.55	0.79	0.47	0.44	**0.99**	0.75	0.90	0.56	0.79	0.51	0.46	**1.03**
18	0.70	0.91	0.64	0.90	0.48	0.50	**1.05**	0.75	0.86	0.55	0.79	0.50	0.44	**1.05**
20	0.75	1.02	0.71	1.02	0.53	0.56	**1.17**	0.67	0.74	0.48	0.68	0.44	0.38	**0.93**

Note: bold values indicate more practical IM.

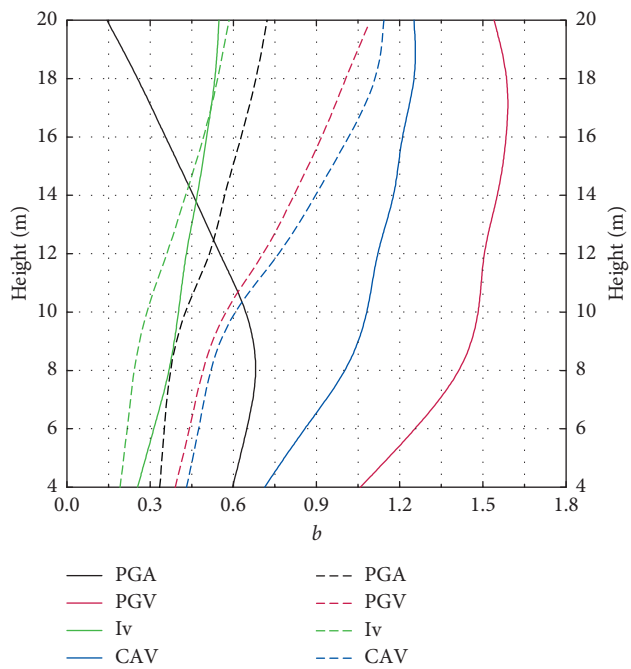

Figure 10: Practicality comparison of IMs under pulse-like and far-field ground motions. The solid lines and dashed lines refer to the cases of pulse-like and far-field ground motions, respectively.

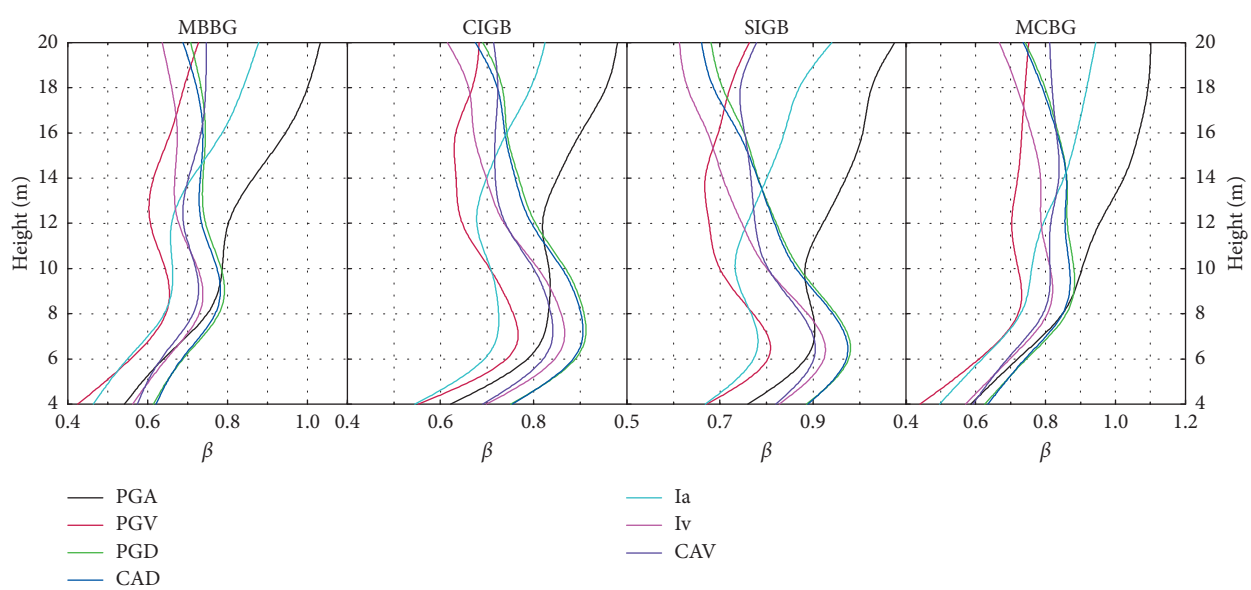

(a)

Figure 11: Continued.

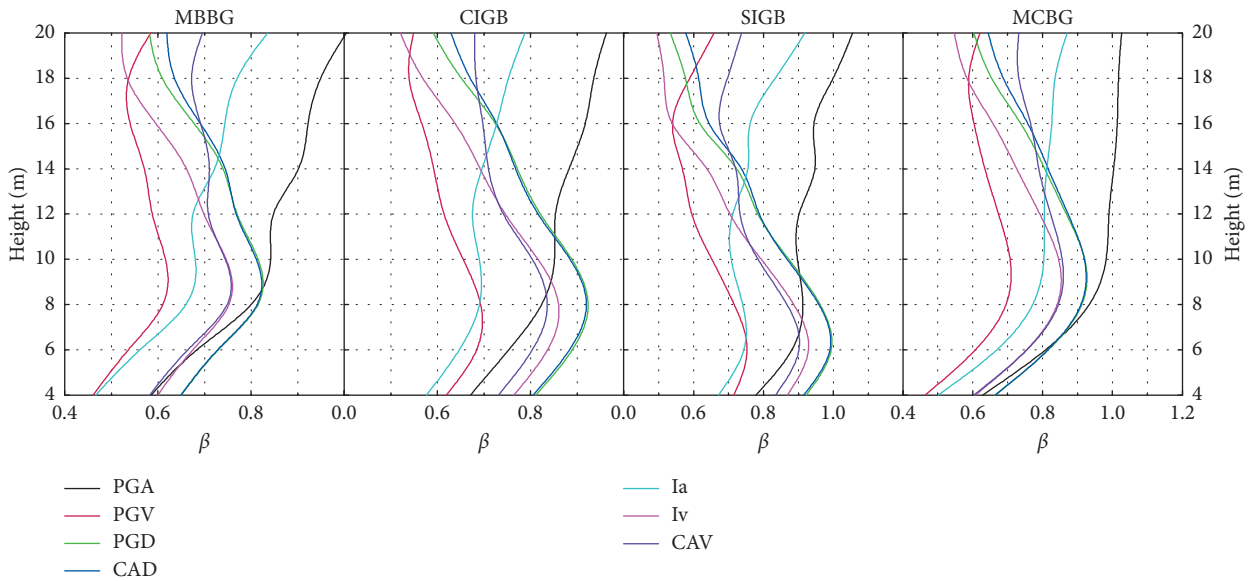

(b)

Figure 11: IMs efficiency comparison for (a) the pier curvature ductility along the longitudinal direction and (b) the pier curvature ductility along the transverse direction.

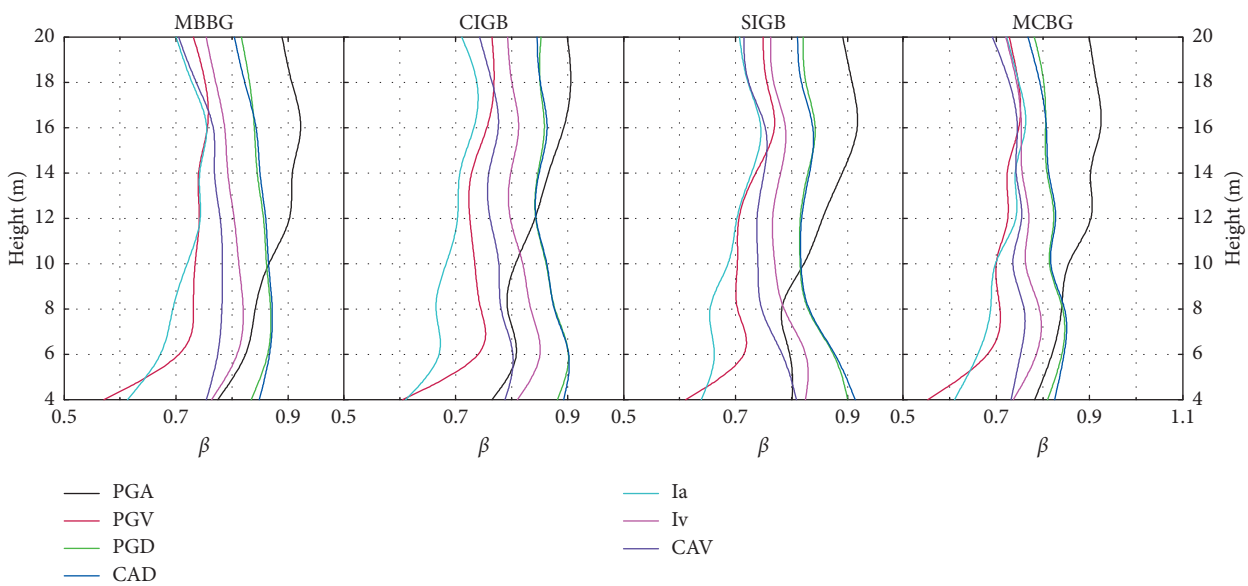

(a)

Figure 12: Continued.

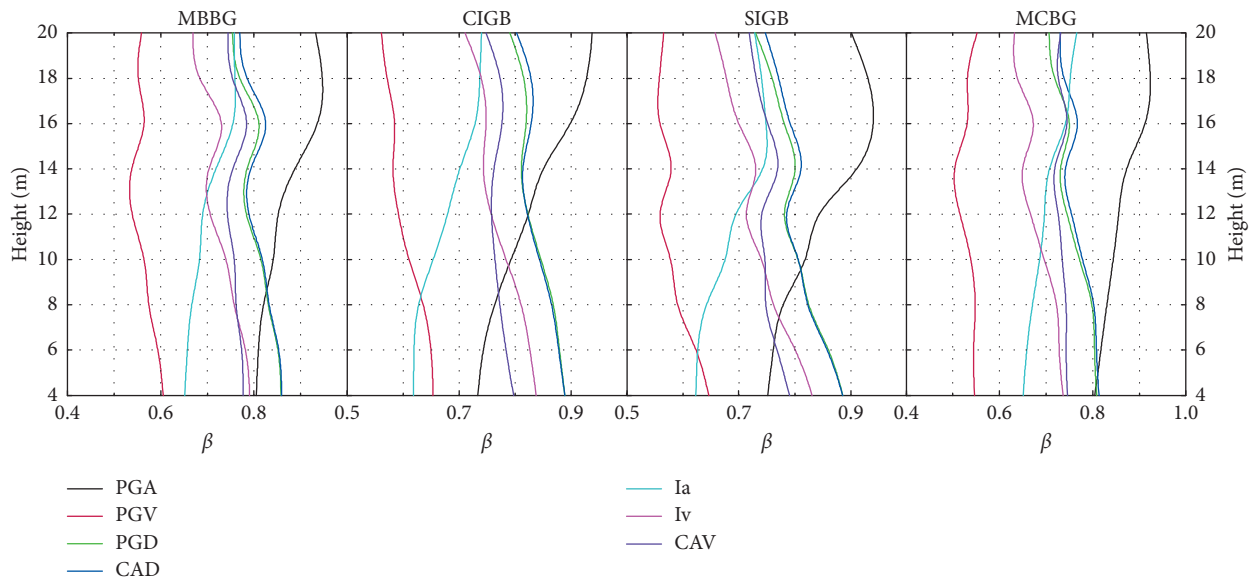

(b)

Figure 12: IMs efficiency comparison for (a) the bearing deformation along the longitudinal direction and (b) the bearing deformation along the transverse direction.

Table 6: Demand models and efficiency comparison of IMs subjected to far-field ground motions.

Height (m)	μ_x							δ_x						
	PGA	PGV	PGD	CAD	Ia	Iv	CAV	PGA	PGV	PGD	CAD	Ia	Iv	CAV
4	0.27	0.22	0.27	0.23	0.23	**0.21**	0.23	0.47	**0.33**	0.53	0.44	0.42	0.35	0.45
6	0.31	0.29	0.36	0.31	0.29	**0.28**	0.29	0.56	**0.47**	0.60	0.54	0.51	0.49	0.53
8	0.38	0.30	0.40	0.33	0.34	**0.30**	0.34	0.60	**0.50**	0.64	0.58	0.55	0.52	0.57
10	0.44	0.37	0.43	0.37	0.40	**0.35**	0.39	0.64	**0.53**	0.65	0.58	0.58	0.54	0.59
12	0.50	0.41	0.48	0.42	0.45	**0.39**	0.43	0.64	0.56	0.67	0.60	0.60	**0.55**	0.60
14	0.56	0.43	0.53	0.46	0.51	**0.41**	0.50	0.61	0.49	0.60	0.53	0.55	**0.47**	0.55
16	0.65	0.51	0.56	0.50	0.59	**0.46**	0.57	0.64	0.49	0.58	0.53	0.58	**0.47**	0.58
18	0.73	0.58	0.59	0.53	0.68	**0.50**	0.65	0.60	0.47	0.54	0.48	0.53	**0.43**	0.51
20	0.82	0.63	0.65	0.56	0.75	**0.53**	0.71	0.53	0.45	0.50	0.45	0.49	**0.42**	0.47

Note: bold values indicate more efficient IM.

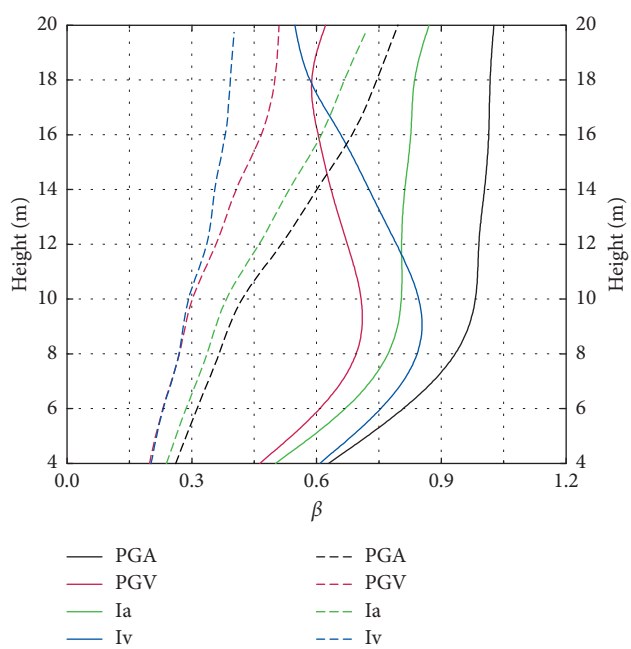

Figure 13: Efficiency comparison of IMs under pulse-like and far-field ground motions. The solid lines and dashed lines refer to the cases under pulse-like and far-field ground motions, respectively.

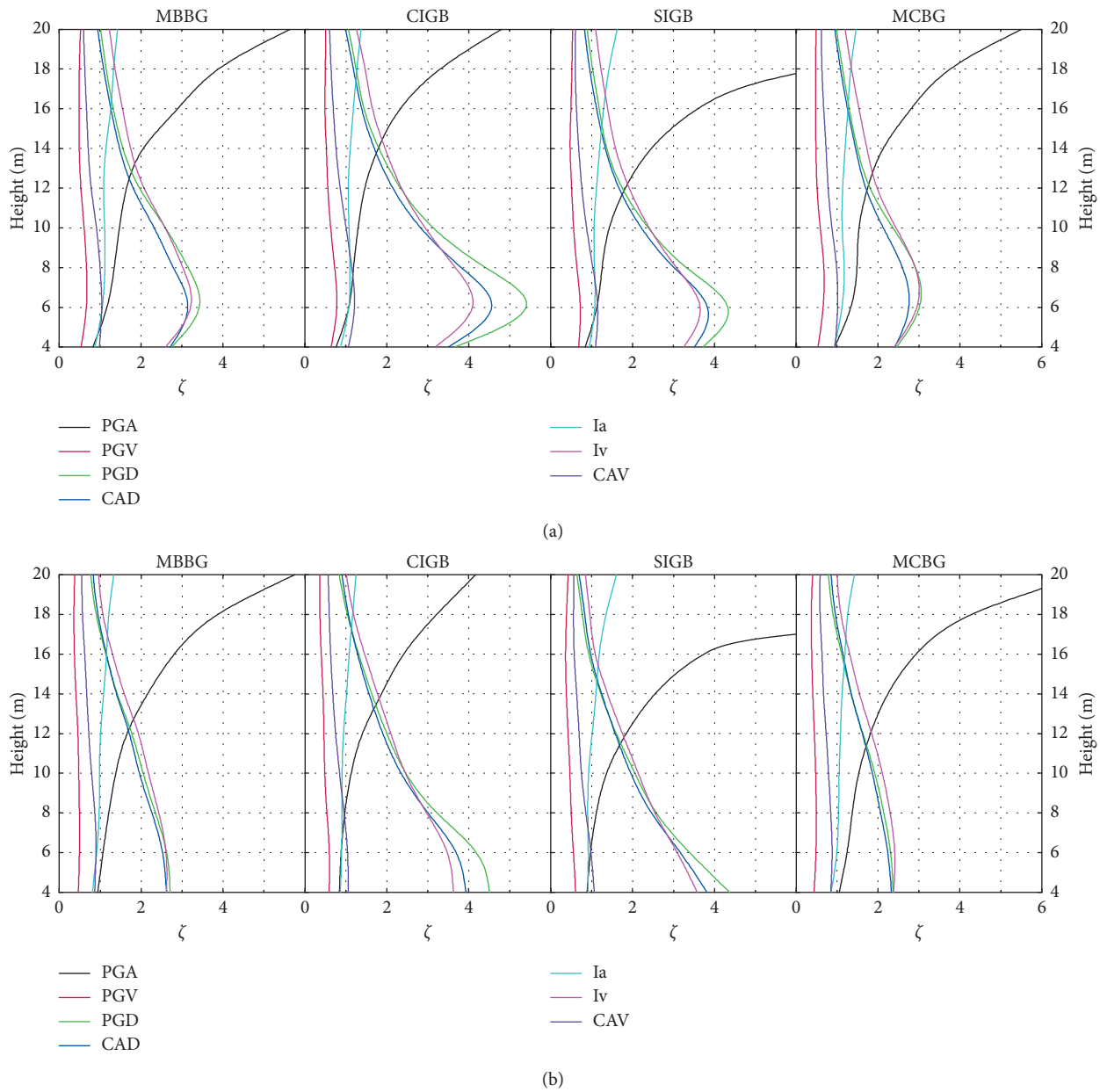

Figure 14: IMs proficiency comparison for (a) the pier curvature ductility along the longitudinal direction and (b) the pier curvature ductility along the transverse direction.

In general, PGV tends to be the most efficient IM. An interesting phenomenon observed is that PGA is not efficient similar to the practicality comparison for the long-period structures, which supports the abovementioned assumption strongly.

Similarly, Table 6 lists the efficiency comparison of the seven structure-independent IMs under far-field ground motions. As shown in the table, Iv tends to be the most efficient IM. For the considered height range, PGA and PGD are less efficient because of relatively large efficiency parameter $\beta_{D|IM}$. Similarly, to demonstrate the pulse effect on the comparison results, Figure 13 shows the efficiency comparison of IMs under pulse-like ground motions and far-field ground motions, where PGA, PGV, Iv, and Ia are chosen as the candidate IMs (conditioning on μ_y, the other cases follow the similar tendency). As shown in the figure, PGV can be chosen as the appropriate IM to predict the seismic response of bridges under either far-field or pulse-like ground motions with respect to efficiency. In addition, PGA is the least efficient IM under either pulse-like or far-field ground motions due to the largest dispersion $\beta_{D|IM}$.

6.3. Proficiency. The composite measure ζ can be utilized to estimate the proficiency of IMs, which combines practicality and efficiency. A more proficient IM has a lower ζ. The proficiency comparison of IMs is given in Figures 14 and 15. As illustrated in the figures, ζ is smaller for PGV

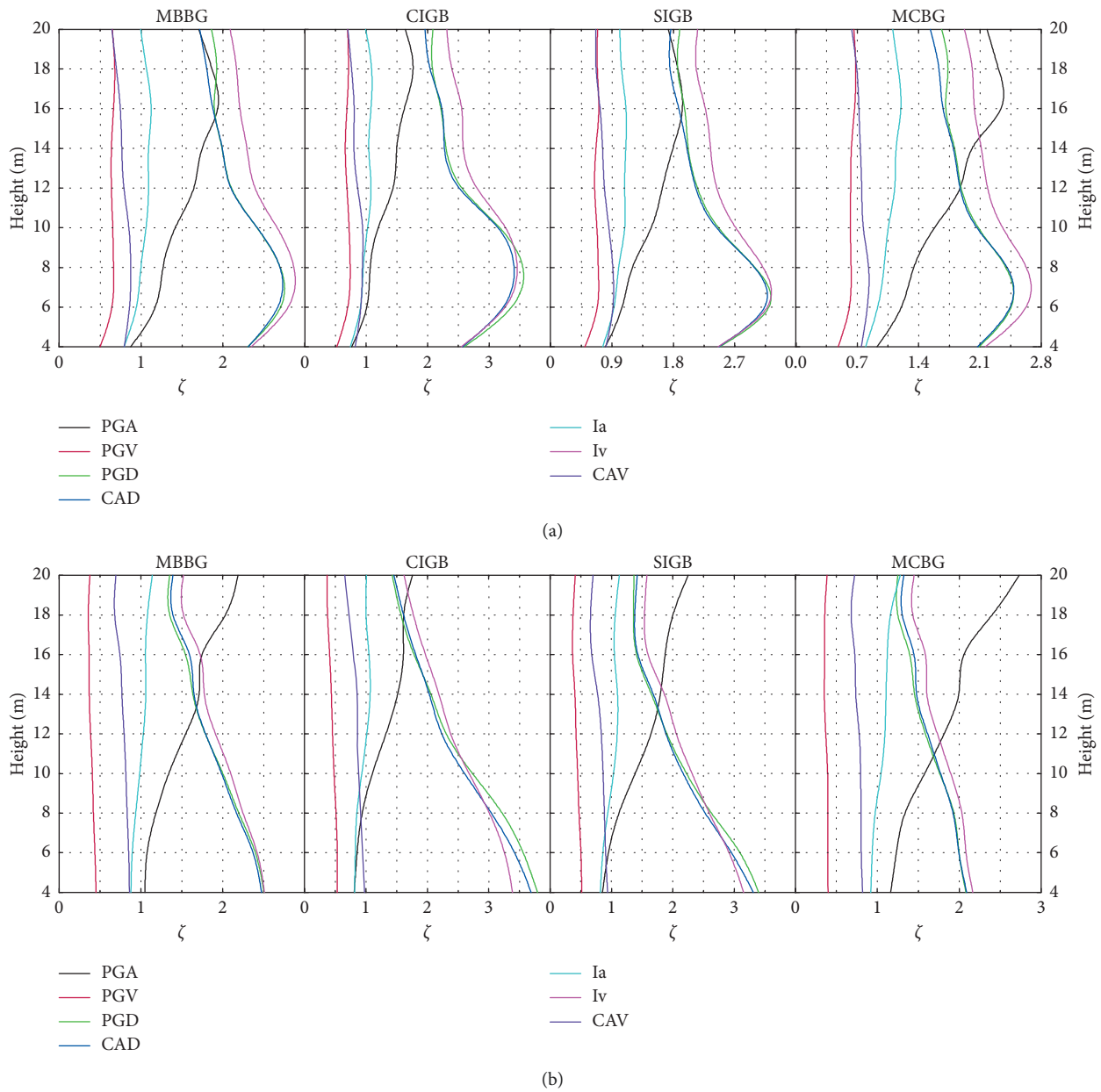

Figure 15: IMs proficiency comparison for (a) the bearing deformation along the longitudinal direction and (b) the bearing deformation along the transverse direction.

Table 7: Demand models and proficiency comparison of IMs subjected to far-field ground motions.

Height (m)	μ_x							δ_x						
	PGA	PGV	PGD	CAD	Ia	Iv	CAV	PGA	PGV	PGD	CAD	Ia	Iv	CAV
4	0.76	0.59	1.06	0.68	1.01	1.08	**0.51**	0.59	**0.40**	1.05	0.62	0.89	0.86	0.50
6	0.77	0.66	1.83	0.86	1.06	1.38	**0.53**	0.79	0.61	1.51	0.88	1.12	1.32	**0.59**
8	0.85	0.58	1.50	0.74	1.13	1.16	**0.54**	0.82	0.62	1.54	0.88	1.16	1.32	**0.61**
10	1.02	0.69	1.40	0.76	1.36	1.27	**0.61**	0.91	0.66	1.48	0.87	1.25	1.35	**0.63**
12	0.91	0.64	1.30	0.72	1.19	1.17	**0.55**	0.85	0.67	1.47	0.83	1.20	1.31	**0.60**
14	0.85	0.54	1.13	0.65	1.15	1.02	**0.53**	0.81	0.57	1.19	0.69	1.09	1.08	**0.54**
16	0.94	0.60	1.03	0.64	1.26	1.04	**0.58**	0.85	0.56	1.05	0.66	1.14	1.02	**0.55**
18	1.05	0.63	0.92	**0.59**	1.40	1.01	0.62	0.80	0.55	0.98	0.60	1.05	0.98	**0.49**
20	1.09	0.62	0.92	**0.55**	1.43	0.96	0.61	0.80	0.61	1.03	0.67	1.10	1.10	**0.51**

Note: bold values indicate more proficient IM.

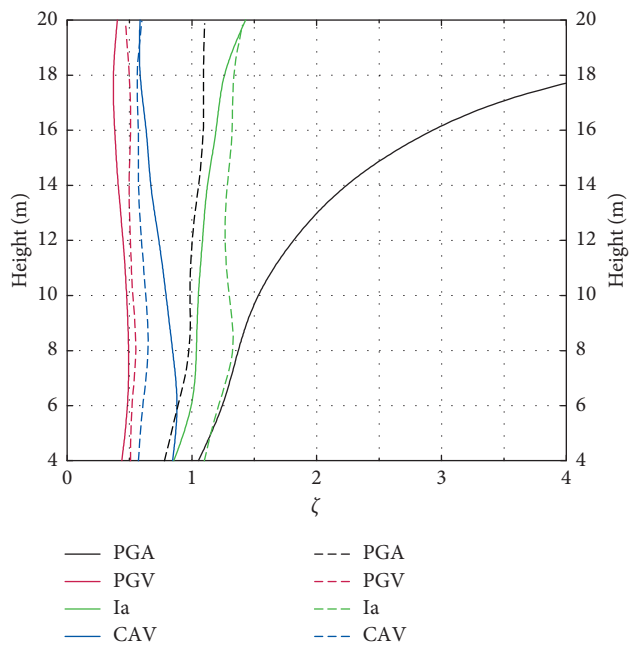

Figure 16: Proficiency comparison of IMs under pulse-like and far-field ground motions. The solid lines and dashed lines refer to the cases of pulse-like and far-field ground motions, respectively.

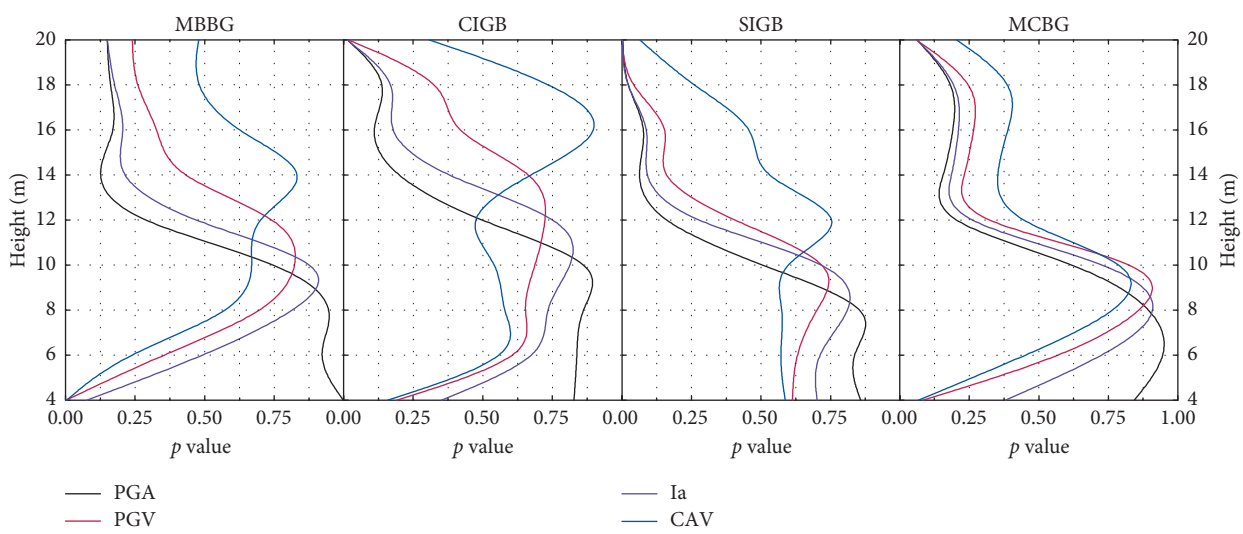

(a)

Figure 17: Continued.

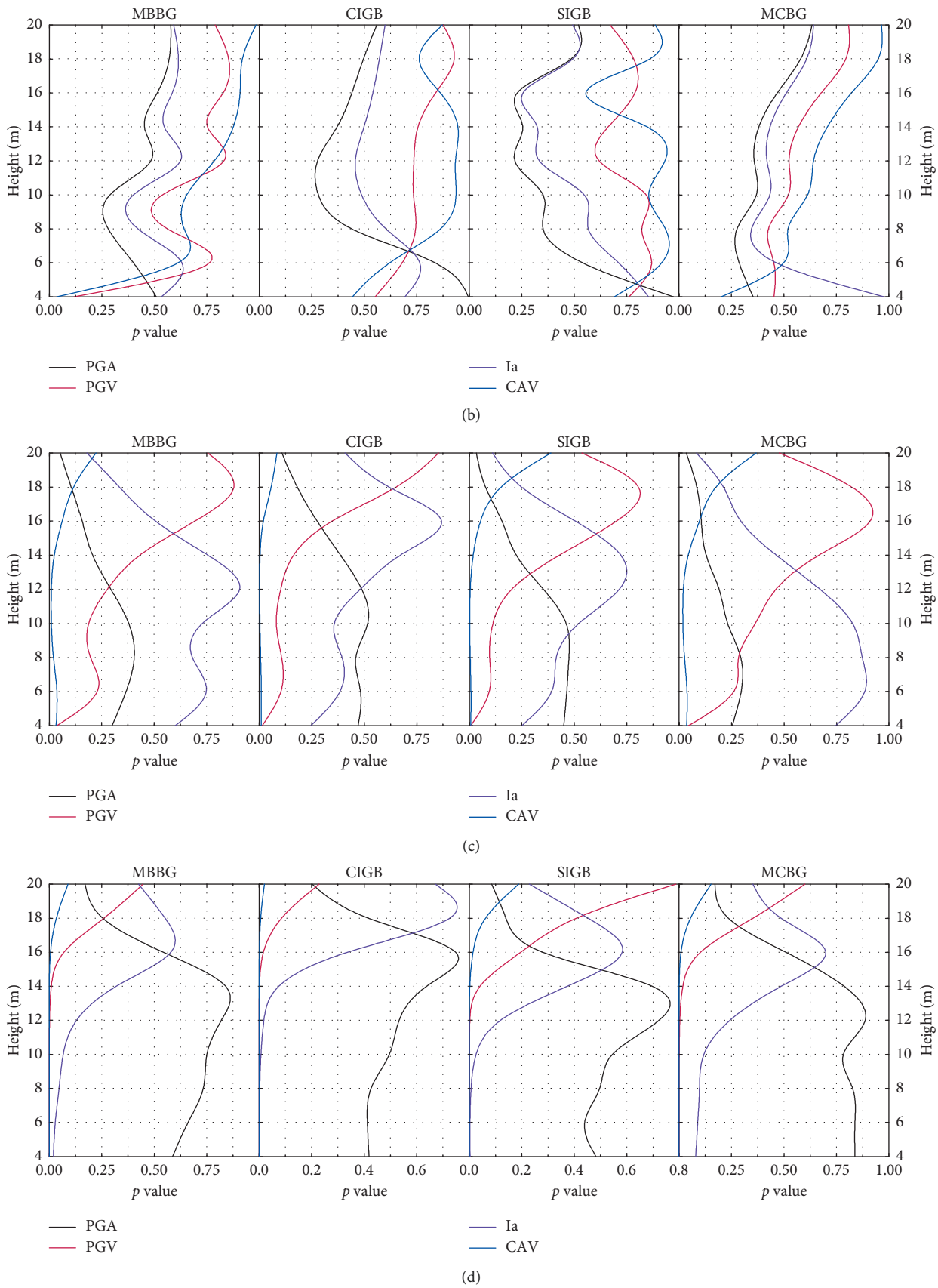

Figure 17: IMs sufficiency comparison with respect to M for (a) the pier curvature ductility along the longitudinal direction, (b) the pier curvature ductility along the transverse direction, (c) the bearing deformation along the longitudinal direction, and (d) the bearing deformation along the transverse direction.

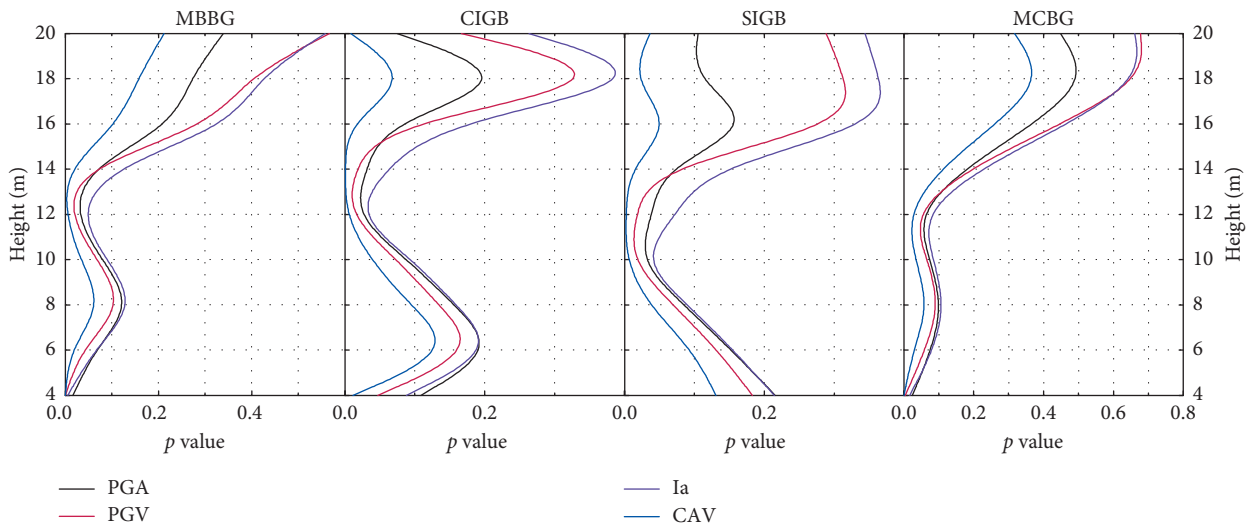

(a)

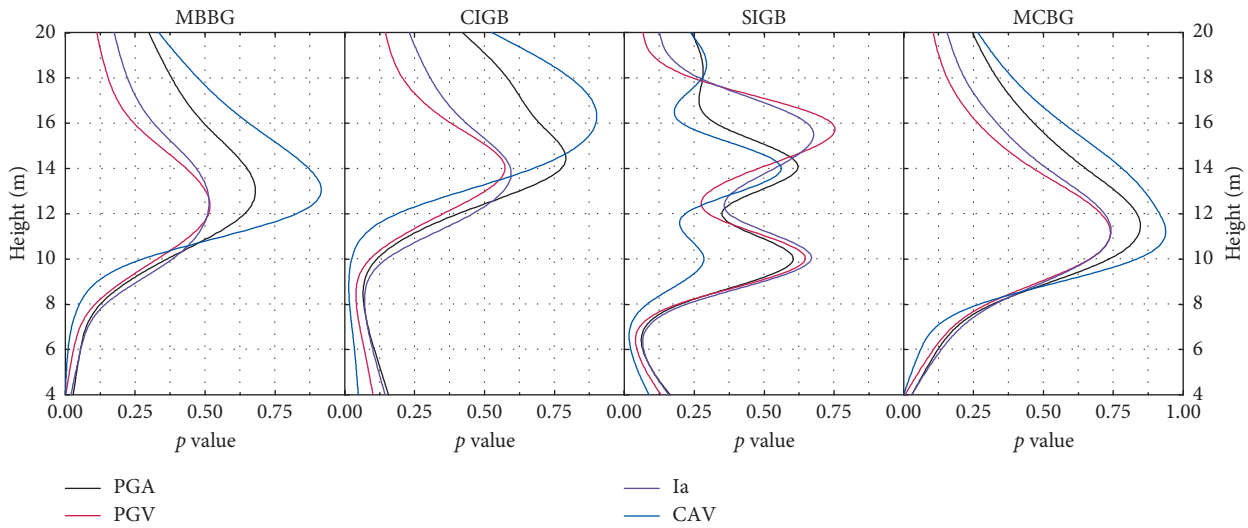

(b)

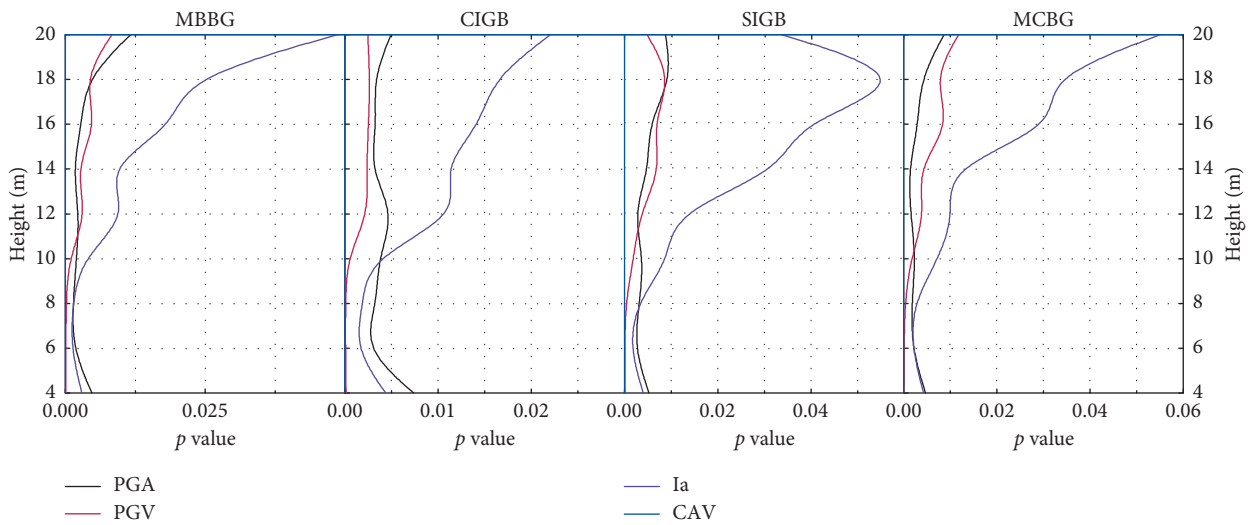

(c)

Figure 18: Continued.

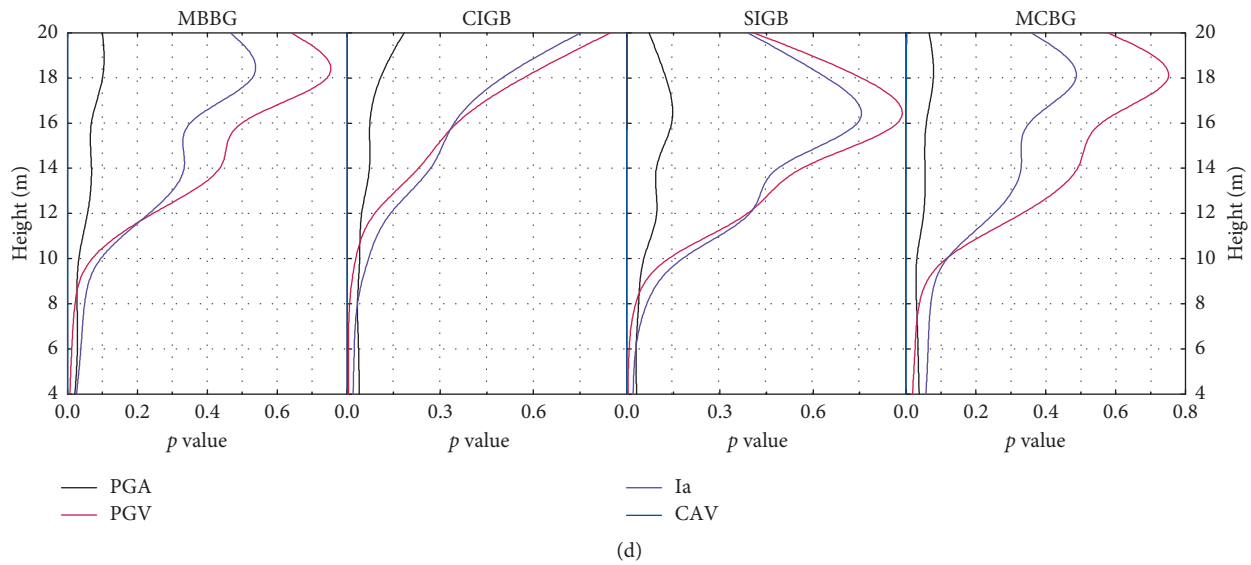

Figure 18: IMs sufficiency comparison with respect to R for (a) the pier curvature ductility along the longitudinal direction, (b) the pier curvature ductility along the transverse direction, (c) the bearing deformation along the longitudinal direction, and (d) the bearing deformation along the transverse direction.

Table 8: Demand models and sufficiency comparison using p values of IMs subjected to far-field ground motions.

	Height (m)	μ_x							δ_x						
		PGA	PGV	PGD	CAD	Ia	Iv	CAV	PGA	PGV	PGD	CAD	Ia	Iv	CAV
M	4	0.18	0.47	0.41	0.79	0.77	0.73	**0.82**	0.14	0.28	0.24	0.85	0.50	**0.97**	0.68
	6	0.05	0.87	0.15	0.92	0.63	0.58	**0.98**	0.03	0.71	0.10	0.47	0.26	**0.87**	0.35
	8	0.02	0.63	0.18	0.65	0.43	0.26	**0.88**	0.06	0.89	0.16	0.62	0.35	**0.95**	0.45
	10	0.01	**0.91**	0.23	0.57	0.26	0.30	0.70	0.05	0.79	0.17	0.64	0.30	**0.97**	0.41
	12	0.01	**0.99**	0.18	0.76	0.25	0.34	0.60	0.06	0.67	0.15	0.60	0.30	**0.95**	0.39
	14	0.01	**0.87**	0.18	0.82	0.17	0.30	0.42	0.01	0.26	0.05	0.24	0.08	**0.43**	0.13
	16	0.002	0.41	0.08	0.62	0.05	0.92	0.12	0.03	0.43	0.13	0.43	0.14	**0.70**	0.20
	18	0.002	0.16	0.04	0.28	0.02	**0.50**	0.06	0.01	0.13	0.05	0.17	0.05	**0.24**	0.09
	20	0.002	0.16	0.03	0.25	0.02	**0.50**	0.05	0.05	0.61	0.28	0.75	0.28	**0.99**	0.45
R	4	0.52	**0.97**	0.47	0.29	0.59	0.85	0.19	0.11	**0.18**	0.04	0.03	0.10	0.13	0.02
	6	0.63	**0.95**	0.10	0.18	0.50	0.65	0.14	0.14	**0.34**	0.02	0.03	0.11	0.16	0.02
	8	0.69	0.52	0.16	0.31	0.64	**0.82**	0.18	0.13	**0.33**	0.02	0.03	0.10	0.16	0.02
	10	0.47	0.76	0.16	0.29	0.44	**0.91**	0.14	0.17	**0.46**	0.04	0.05	0.15	0.27	0.04
	12	0.45	0.77	0.13	0.22	0.43	**0.95**	0.10	0.31	**0.60**	0.08	0.09	0.27	0.41	0.08
	14	0.37	0.65	0.11	0.18	0.33	**0.93**	0.07	0.25	**0.55**	0.09	0.10	0.23	0.39	0.08
	16	0.23	**0.92**	0.09	0.10	0.21	0.80	0.05	0.10	**0.26**	0.03	0.03	0.09	0.16	0.03
	18	0.24	0.83	0.18	0.17	0.26	**0.88**	0.11	0.25	**0.47**	0.16	0.18	0.25	0.44	0.14
	20	0.20	0.78	0.13	0.12	0.22	**0.84**	0.10	0.19	**0.38**	0.07	0.08	0.16	0.30	0.06

Note: bold values indicate more sufficient IM.

conditioning on the curvature ductility and bearing deformation in the longitudinal and transverse directions, which indicates that PGV is the most proficient IM, followed by CAV. For the considered height range, Iv, CAD, PGD, and PGA tend to be less appropriate because of the relatively high proficiency parameters ζ. Similarly, for long-period cases, PGA is not a proficient IM, which is consistent with the practicality and efficiency comparison results. This phenomenon reveals that PGA is not appropriate to be chosen as the IM to develop PSDMs of long-period structures under pulse-like ground motions.

Similarly, Table 7 summarizes the proficiency comparison of the seven structure-independent IMs under far-field ground motions. As shown in the table, CAV tends to be the most proficient IM, followed by PGV. To demonstrate the pulse effect on the comparison results, Figure 16 shows the proficiency comparison of IMs under pulse-like ground motions and far-field ground motions, where PGA, PGV, CAV, and Ia are chosen as the candidate IMs (conditioning on μ_y, the other cases follow the similar tendency). As shown in the figure, PGV can be chosen as the appropriate IM to assess the seismic demand under both far-field and pulse-like ground motions with respect to proficiency. In addition, PGA is less appropriate to perform the vulnerability analysis under either pulse-like or far-field ground motions because of the relatively large ζ. One should notice that ζ value of

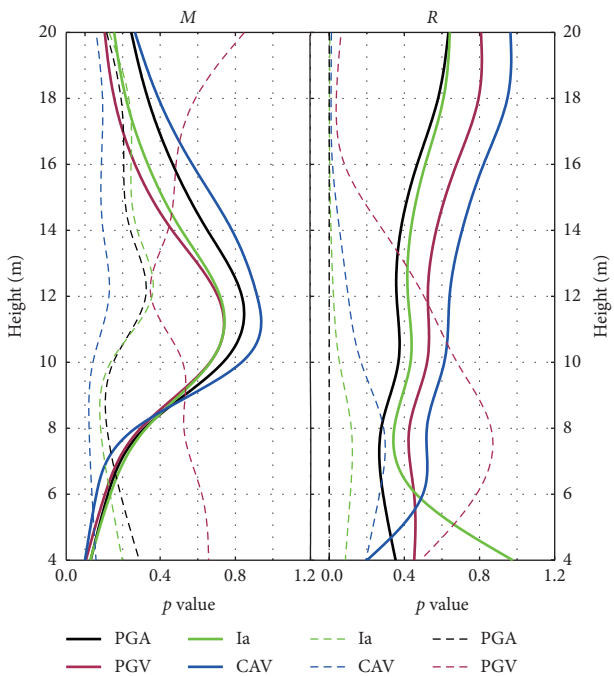

Figure 19: Sufficiency comparison of IMs under pulse-like and far-field ground motions. The solid lines and dashed lines refer to the cases under pulse-like and far-field ground motions, respectively.

PGA increases extremely with the height of pier under pulse-like ground motions, which reveals that PGA is the least proficient under pulse-like ground motions. This phenomenon is consistent with the practicality and efficiency comparison results.

6.4. Sufficiency. The p value, which is obtained with a regression analysis on the residual, ε/IM, from the PSDM relative to the ground motion characteristics, that is, M or R, is an indicator of sufficiency of IMs. Generally, the p value of 0.1 is regarded as the cutoff of an insufficient IM.

A larger p value signifies that the IM is more sufficient. The sufficiency comparison of the four candidate IMs, namely, PGV, PGA, CAV, and Ia, is given in Figures 17 and 18. As indicated in the figures, PGA tends to be the most sufficient IM conditioning on the pier curvature ductility for the lower height range (from 4 m to 6 m) with respect to M and R in the longitudinal and transverse directions. For the higher height cases (larger than 8 m), CAV tends to more sufficient, followed by PGV. For the displacement-related EDP, namely, bearing deformation, PGA tends to be the most sufficient IM for the lower height cases (4 m to 8 m) with respect to M; with height increasing, PGV is more sufficient. However, CAV tends to be the most sufficient IM with respect to R for the lower height range (4 m to 8 m) in the longitudinal and transverse directions. As height increases, CAV and PGV tend to be the most sufficient IMs in the longitudinal and transverse directions, respectively. In general, both PGA and PGV can be selected as the most sufficient IMs for PSDMs of isolated bridges.

Similarly, Table 8 shows the sufficiency comparison of the seven structure-independent IMs under far-field ground motions. As shown in the table, Iv tends to be the most sufficient IM, followed by PGV and CAV. To demonstrate the pulse influence on the sufficiency comparison results, Figure 19 shows the sufficiency comparison of IMs under pulse-like ground motions and far-field ground motions, where PGA, PGV, CAV, and Ia are chosen as the candidate IMs (conditioning on μ_y, the other cases follow the similar tendency). As shown in the figure, PGV is found to be more sufficient with respect to R and less sufficient with respect to M under pulse-like ground motions. Under far-field ground motions, PGV is appropriately independent of M and R. Similarly, PGA is relatively dependent on M and R, which implies that PGA is less sufficient.

In general, based on the practicality, efficiency, proficiency, and sufficiency comparison results, PGV can be selected as the optimal IM to assess the seismic demand of isolated bridges under pulse-like and far-field ground motions. However, PGA is not an appropriate IM to establish PSDMs of isolated bridges, which is commonly used in the fragility analysis of structures.

7. Conclusion

The intensity measure (IM) plays a vital role in linking the seismic hazard analysis with the structural demand (e.g., curvature ductility and bearing deformation). Traditional ground motion models used in the probabilistic seismic hazard demand analysis do not account for pulse effect and may underestimate the seismic demand of structures located in the near-fault region. In addition, the research of the optimal intensity measure selection targeted at pulse-like ground motions is rare and there is no widely accepted optimal intensity measure for pulse-like ground motions in the bridge engineering community, which emphasizes the necessity of the research of optimal intensity measures targeted at the pulse-like ground motions.

The objective of this paper is to identify the optimal IM of PSDMs for isolated bridges subjected to pulse-like ground motions. For this purpose, we select four common isolated girder bridge types with varied pier height (from 4 m to 20 m), that is, multicell box girder (MCBG), multibeam box girder (MBBG), concrete I-girder bridge (CIGB), and steel I-girder bridge (SIGB), as case studies. Totally seven structure-independent IMs, namely, peak ground acceleration (PGA), peak ground velocity (PGV), peak ground displacement (PGD), Arias intensity (Ia), velocity intensity (Iv), cumulative absolute velocity (CAV), and cumulative absolute displacement (CAD), are selected as the candidate IMs. The probabilistic seismic demand analysis is performed using 121 pairs of pulse-like ground motions. The engineering demand parameters (EDPs), namely, pier curvature ductility (μ_x, μ_y) and bearing deformation (δ_x, δ_y), are monitored and reordered. Efficiency, practicality, proficiency, sufficiency, and hazard computability are selected as the selection metrics of an optimal intensity measure.

In general, PGV tends to be the optimal IM for conditioning PSDMs of isolated bridges with the considered pier height range based on the five metrics mentioned above. This phenomenon can be explained in that the response of isolated bridges under pulse-like ground motions is

dominated by the pulse characteristic. In addition, as a commonly used IM, PGA is not an appropriate choice to establish the fragility curves of isolated bridges under pulse-like ground motions, which signifies that special attention should be paid to the intensity measure selection when the pulse effect cannot be ignored. The results obtained in this paper are intended to offer guidance for probabilistic seismic demand analysis of isolated bridges near the fault.

Data Availability

All data, models, and codes generated or used during the study are available from the corresponding author upon request.

Conflicts of Interest

The authors declare that they have no conflicts of interest.

Acknowledgments

This research was supported by the National Natural Science Foundation of China (51608161 and 51778471), the China Postdoctoral Science Foundation (2016M602007), the Fundamental Research Funds for the Central Universities of China (PA2019GDPK0041), and the Ministry of Science and Technology of China (SLDRCE19-B-19). The supports are gratefully acknowledged.

References

[1] J. Zhong, J.-S. Jeon, Y.-H. Shao, W. Yuan, and L. Chen, "Optimal intensity measures in probabilistic seismic demand models of cable-stayed bridges subjected to pulse-like ground motions," *Journal of Bridge Engineering*, vol. 24, no. 2, 2019.

[2] J. W. Baker, "Quantitative classification of near-fault ground motions using wavelet analysis," *Bulletin of the Seismological Society of America*, vol. 97, no. 5, pp. 1486–1501, 2007.

[3] V. V. Bertero, R. A. Herrera, and S. A. Mahin, "Establishment of design earthquakes-evaluation of present methods," in *Proceedings of the International Symposium on Earthquake Structural Engineering*, St Louis, MO, USA, August 1976.

[4] V. V. Bertero, S. A. Mahin, and R. A. Herrera, "Aseismic design implications of near-fault san fernando earthquake records," *Earthquake Engineering & Structural Dynamics*, vol. 6, no. 1, pp. 31–42, 1978.

[5] P. G. Somerville and N. A. Abrahamson, "Accounting for near-fault rupture directivity effects on the development of design ground motions," in *Proceedings of the 11th World Conference on Earthquake Engineering*, Acapulco, Mexico, June 1996.

[6] Y. Bozorgnia and S. A. Mahin, "Ductility and strength demands of near-fault ground motions of the Northridge earthquake," in *Proceedings of the 6th U.S. National Conference on Earthquake Engineering*, Seattle, DC, USA, 1998.

[7] J. E. Padgett, B. G. Nielson, and R. DesRoches, "Selection of optimal intensity measures in probabilistic seismic demand models of highway bridge portfolios," *Earthquake Engineering & Structural Dynamics*, vol. 37, no. 5, pp. 711–725, 2008.

[8] ATC, *Earthquake Damage Evaluation Data for California ATC-13*, Applied Technology Council, Redwood City, CA, USA, 1985.

[9] X. Wang, A. Ye, A. Shafieezadeh, and J. E. Padgett, "Fractional order optimal intensity measures for probabilistic seismic demand modeling of extended pile-shaft-supported bridges in liquefiable and laterally spreading ground," *Soil Dynamics and Earthquake Engineering*, vol. 120, pp. 301–315, 2019.

[10] X. Wang, A. Shafieezadeh, and A. Ye, "Optimal intensity measures for probabilistic seismic demand modeling of extended pile-shaft-supported bridges in liquefied and laterally spreading ground," *Bulletin of Earthquake Engineering*, vol. 16, no. 1, pp. 229–257, 2018.

[11] J. W. Baker and C. A. Cornell, "A vector-valued ground motion intensity measure consisting of spectral acceleration and epsilon," *Earthquake Engineering & Structural Dynamics*, vol. 34, no. 10, pp. 1193–1217, 2005.

[12] K. G. Kostinakis and A. M. Athanatopoulou, "Evaluation of scalar structure-specific ground motion intensity measures for seismic response prediction of earthquake resistant 3D buildings," *Earthquakes and Structures*, vol. 9, no. 5, pp. 1091–1114, 2015.

[13] J. K. Mackie and B. Stojadinovic, "Fragility curves for reinforced concrete highway overpass bridges," in *Proceedings of the 3th World Conference on Earthquake Engineering*, Wellington, New Zealand, 2004.

[14] D. Yang, J. Pan, and G. Li, "Non-structure-specific intensity measure parameters and characteristic period of near-fault ground motions," *Earthquake Engineering & Structural Dynamics*, vol. 38, no. 11, pp. 1257–1280, 2009.

[15] M. Yakhchalian, A. Nicknam, and G. G. Amiri, "Proposing an optimal integral-based intensity measure for seismic collapse capacity assessment of structures under pulse-like near-fault ground motions," *Journal of Vibroengineering*, vol. 16, no. 3, pp. 1360–1375, 2014.

[16] J. W. Baker and C. A. Cornell, "Vector-valued intensity measures incorporating spectral shape for prediction of structural response," *Journal of Earthquake Engineering*, vol. 12, no. 4, pp. 534–554, 2008.

[17] H. Li, W.-J. Yi, and X.-X. Yuan, "Fuzzy-valued intensity measures for near-fault pulse-like ground motions," *Computer-Aided Civil and Infrastructure Engineering*, vol. 28, no. 10, pp. 780–795, 2013.

[18] N. Luco and C. A. Cornell, "Structure-specific scalar intensity measures for near-source and ordinary earthquake ground motions," *Earthquake Spectra*, vol. 23, no. 2, pp. 357–392, 2007.

[19] K. Mackie and B. Stojadinović, "Probabilistic seismic demand model for California highway bridges," *Journal of Bridge Engineering*, vol. 6, no. 6, pp. 468–481, 2001.

[20] P. Giovenale, C. A. Cornell, and L. Esteva, "Comparing the adequacy of alternative ground motion intensity measures for the estimation of structural responses," *Earthquake Engineering & Structural Dynamics*, vol. 33, no. 8, pp. 951–979, 2004.

[21] Ministry of Transport of the People's Republic of China, *Guidelines for Seismic Design of Highway Bridges, JTG/T B02-01-2008*, Ministry of Transport of the People's Republic of China, Beijing, China, 2008.

[22] J. Zhang and Y. Huo, "Evaluating effectiveness and optimum design of isolation devices for highway bridges using the fragility function method," *Engineering Structures*, vol. 31, no. 8, pp. 1648–1660, 2009.

[23] Ministry of Transport of the People's Republic of China, *Lead Rubber Bearing Isolator for Highway Bridge, JT/T 822-2011*, Ministry of Transport of the People's Republic of China, Beijing, China, 2011.

[24] F. Mckenna, M. H. Scott, and G. L. Fenves, "Nonlinear finite-element analysis software architecture using object composition," *Journal of Computing in Civil Engineering*, vol. 24, no. 1, pp. 95–107, 2010.

[25] D. C. Kent and D. Park, "Flexural members with confined concrete," *Journal of Structure Division*, vol. 97, no. 7, pp. 1969–1990, 1971.

[26] J. E. Luco and A. Lanzi, "Numerical artifacts associated with Rayleigh and modal damping models of inelastic structures with massless coordinates," *Earthquake Engineering & Structural Dynamics*, vol. 48, no. 13, pp. 1491–1507, 2019.

[27] S. Castellaro, "Soil and structure damping from single station measurements," *Soil Dynamics and Earthquake Engineering*, vol. 90, pp. 480–493, 2016.

[28] S. K. Shahi and J. W. Baker, "An empirically calibrated framework for including the effects of near-fault directivity in probabilistic seismic hazard analysis," *Bulletin of the Seismological Society of America*, vol. 101, no. 2, pp. 742–755, 2011.

[29] M. Dabaghi and A. D. Kiureghian, "Stochastic model for simulation of near-fault ground motions," *Earthquake Engineering & Structural Dynamics*, vol. 46, no. 6, pp. 963–984, 2017.

[30] A. Shafieezadeh, K. Ramanathan, J. E. Padgett, and R. DesRoches, "Fractional order intensity measures for probabilistic seismic demand modeling applied to highway bridges," *Earthquake Engineering & Structural Dynamics*, vol. 41, no. 3, pp. 391–409, 2012.